Short title: GWAS/TWAS of stomatal closure in biomass sorghum

Corresponding author: Andrew D. B. Leakey: 217-244-0302, leakey@illinois.edu

Full title: Phenotyping stomatal closure by thermal imaging for GWAS and TWAS of water use efficiency-related genes

Charles P. Pignon[1,2,3], Samuel B. Fernandes[2,3], Ravi Valluru[4,5], Nonoy Bandillo[4,6], Roberto Lozano[7], Edward Buckler[7,8], Michael A. Gore[7], Stephen P. Long[1,2,3,9], Patrick J. Brown[2,3], Andrew D. B. Leakey[1,3,4]

Affiliations:

[1]Department of Plant Biology, University of Illinois at Urbana-Champaign, Urbana, IL 61801, USA.

[2]Department of Crop Sciences, University of Illinois at Urbana-Champaign, Urbana, IL 61801, USA.

[3]Carl R. Woese Institute for Genomic Biology, University of Illinois at Urbana-Champaign, Urbana, IL 61801, USA.

[4]Institute for Genomic Diversity, Cornell University, Ithaca, NY 14853, USA.

[5]Lincoln Institute for Agri-Food Technology, University of Lincoln, LN1 3QE Lincoln, UK.

[6]Department of Plant Sciences, North Dakota State University, Fargo, ND 58105, USA.

[7]Plant Breeding and Genetics Section, School of Integrative Plant Science, Cornell University, Ithaca, NY 14853, USA

[8]United States Department of Agriculture, Agricultural Research Service (USDA-ARS) R.W. Holley Center for Agriculture and Health, Ithaca, NY 14853, USA

[9]Lancaster Environment Centre, University of Lancaster, LA1 1YX, UK.

ORCIDs: 0000-0002-4237-1649 (C.P.P), 0000-0001-6896-8024 (M.A.G.), 0000-0003-1332-711X (P.J.B.), 0000-0001-6251-024X (A.D.B.L)

One sentence summary:

Rapid phenotyping of 659 accessions of *Sorghum bicolor* revealed heritable stomatal responses to a decrease in light. GWAS/TWAS was used to identify candidate genes influencing traits important to WUE.

Footnotes:

The research was conceived by C.P., S.L., E.B., M.G. and A.L. Experiments were performed by C.P., P.B. and R.V.. Data was analyzed and interpreted by C.P., S.F., R.V., N.B., R.L. and A.L.. C.P. and A.L. wrote the paper with input from all authors. A.L. agrees to serve as the author responsible for contact and ensuring communication.

This research was funded by the Advanced Research Projects Agency-Energy (ARPA-E), U.S. Department of Energy (DOE), under Award Number DE-AR0000661 and the Office of

Biological and Environmental Research in the DOE Office of Science (DE-SC0018277). The views and opinions of authors expressed herein do not necessarily state or reflect those of the United States Government or any agency thereof.

Current addresses:

Pignon C: Benson Hill, 1005 N Warson Rd, St. Louis, MO 63132

Brown P: Department of Plant Sciences, University of California, Davis, CA 95616, USA.

Author for contact: leakey@illinois.edu

This manuscript is submitted as a Research Article

Abstract

Stomata allow CO_2 uptake by leaves for photosynthetic assimilation at the cost of water vapor loss to the atmosphere. The opening and closing of stomata in response to fluctuations in light intensity regulate CO_2 and water fluxes and are essential to maintenance of water-use efficiency (WUE). However, little is known about the genetic basis for natural variation in stomatal movement, especially in C_4 crops. This is partly because the stomatal response to a change in light intensity is difficult to measure at the scale required for association studies. High-throughput thermal imaging was used to bypass the phenotyping bottleneck and assess 10 traits describing stomatal conductance (g_s) before, during and after a stepwise decrease in light intensity for a diversity panel of 659 sorghum accessions. Results from thermal imaging significantly correlated with photosynthetic gas-exchange measurements. g_s traits varied substantially across the population and were moderately heritable (h^2 up to 0.72). An integrated genome-wide and transcriptome-wide association study (GWAS/TWAS) identified candidate genes putatively driving variation in stomatal conductance traits. Of the 239 unique candidate genes identified with greatest confidence, 77 were orthologs of Arabidopsis genes related to functions implicated in WUE, including stomatal opening/closing (24 genes), stomatal/epidermal cell development (35 genes), leaf/vasculature development (12 genes), or chlorophyll metabolism/photosynthesis (8 genes). These findings demonstrate an approach to finding genotype-to-phenotype relationships for a challenging trait as well as candidate genes for further investigation of the genetic basis of WUE in a model C_4 grass for bioenergy, food, and forage production.

Introduction

Water availability is a major limiting factor to agriculture worldwide (Boyer, 1982), and is predicted to become even more limiting due to rising demand for water resulting from increasing atmospheric vapor pressure deficit (VPD) with climate change (Lobell et al., 2008; WWAP, 2015; FAO et al., 2018). Greater crop water use associated with greater above-ground biomass has also been implicated in past and future increases in crop yield (Sinclair et al., 1984; Ray et al., 2013; Lobell et al., 2014; Ort and Long, 2014; Koester et al. 2016; DeLucia et al., 2019). Therefore, unless WUE is enhanced, agricultural systems in the near future will be increasingly threatened by drought, and unsustainable practices such as over-irrigation may result (DeLucia et al., 2019; Leakey et al., 2019).

WUE is key to terrestrial plant growth due to the inherent trade-off between net photosynthetic carbon assimilation (A) and water loss through transpiration (Wong et al., 1979). Most leaf water and CO_2 fluxes pass through stomatal pores (Kerstiens, 1996; Hetherington and Woodward, 2003). Stomatal aperture is dynamically regulated by the movement of stomatal guard cells (Assmann and Jegla, 2016), which respond to extrinsic and intrinsic signals to optimize CO_2 uptake relative to water vapor loss (Medlyn et al 2011). The synchrony of stomatal opening and closing with fluctuations in photosynthetic CO_2 assimilation varies within and among species, with significant consequences for intrinsic water-use efficiency (*iWUE*, the ratio of A to stomatal conductance to water vapor (g_s)) (Lawson and Blatt, 2014; Kaiser et al., 2015). If conditions are favorable for A, but g_s is low, A will be limited by CO_2 supply. Conversely, if A is low, but g_s is high, unnecessary transpiration will occur with no corresponding benefit to A, substantially decreasing *iWUE*. This is important in fluctuating light environments such as field crop canopies, where the movement of clouds and leaves cause frequent and abrupt changes in photosynthetic photon flux density (PPFD) at the leaf level (Pearcy, 1990; Zhu et al., 2004; Way and Pearcy, 2012; Wang et al., 2020).

Generally, g_s responds an order of magnitude more slowly than A to a decline in PPFD, declining to a new steady-state over the course of several minutes (Hetherington and Woodward, 2003; McAusland et al., 2016). This results in a de-synchronization of A and g_s and loss of *iWUE*. Ensuring that A and g_s are synchronized in their response to fluctuating light, by

accelerating stomatal movement, could yield substantial benefits to *iWUE* of 20-30% (Lawson and Blatt, 2014). Proof-of-concept from transgenic manipulation of the stomatal light-sensing mechanism has led to accelerated stomatal movement and improved *iWUE* in fluctuating light in Arabidopsis and tobacco (Glowacka et al., 2018; Papanatsiou et al., 2019). Still, accelerating stomatal movement by breeding or biotechnology for improved *iWUE* remains an open challenge in cereal crops (Faralli et al., 2019).

The genetic basis for natural variation in traits describing stomatal opening/closing is poorly understood, in part because such traits are difficult to phenotype at the scale required for association studies. The response of g_s to fluctuating light is lengthy, with some species needing >30 minutes to transition from steady-state at one light intensity to another (Lawson and Blatt, 2014; McAusland et al., 2016; Deans et al., 2019). The standard measurement of g_s using gas-exchange chambers or porometers requires a single instrument for each leaf, so is costly in terms of personnel and equipment. Using thermal imaging to track changes in leaf temperature resulting from stomatal movement, with the leaf warming up as stomata close due to a proportionate reduction of cooling by transpiration, provides a high throughput phenotyping method in which numerous leaves can be measured simultaneously (Jones et al., 2002; Guilioni et al., 2008; Vialet-Chabrand and Lawson, 2019). Thermal imaging has been used to monitor stomatal closure (Jones et al., 2002) and stress response (Grant et al., 2007) in a grapevine field, to identify Arabidopsis mutants with altered g_s (Merlot et al., 2002), and coupled with chlorophyll fluorescence measurements to screen Arabidopsis plants for *iWUE* (McAusland et al., 2013). In a broad validation experiment, thermal measurements predicted g_s for a range of species exposed to different experimental treatments (Grant et al., 2006). Finally, thermal imaging was used to perform high-throughput phenotyping of the response of hundreds of ecotypes of Arabidopsis to changing light and [CO_2] (Takahashi et al., 2015). However, the ability of thermal imaging to produce trait estimates with sufficiently high heritability to support quantitative genetic investigation of genotype-to-phenotype relationships for stomatal opening/closing remains unclear.

Genome-wide association studies (GWAS) are widely used to identify the genetic basis for natural variation in agronomic, developmental, physiological and biochemical traits in plant species, including sorghum (Casa et al., 2008; Morris et al., 2013; Burks et al., 2015; Ortiz et al.,

2017). The benefits and limitations of the approach have been reviewed in many contexts (Liu and Yan, 2019; Tam et al., 2019; Zhou and Huang, 2019). GWAS of stomatal movement can be challenging because biophysical trade-offs can limit the extent of natural variation in the trait, and because measurements may be slow, sensitive to environmental conditions, and lack accuracy, precision or both. Together, these factors can reduce the variance that can be ascribed to genotype, i.e. reduce heritability, and constrain the size of the mapping population that can be studied, resulting in low statistical power. Recently, combining GWAS with transcriptome-wide association study (TWAS), which identifies significant associations between trait variation and RNA transcript abundance across all expressed genes in a tissue, has been shown to improve identification of genes underlying trait variation (Kremling et al., 2019).

This study aimed to demonstrate how phenotyping by thermal imaging could be used in conjunction with integrated GWAS/TWAS to quantify natural diversity in stomatal/opening closing and identify genotype-to-phenotype relationships in a model C_4 crop. *Sorghum bicolor* ((L.) Moench) is a model species used to study photosynthesis, abiotic/biotic stress and canopy architecture, as well as applied investigations in the context of food, fuel and forage production (Paterson et al., 2009; Morris et al., 2013). It has particular importance in semi-arid conditions due to its high productivity and drought-tolerance (Regassa and Wortmann, 2014; Hadebe et al., 2017). Sorghum is an especially interesting model in which to study stomatal movement because it has fast stomatal responses to decreasing light relative to other species (McAusland et al., 2016; Pignon et al., 2021). High-throughput thermal imaging was used to measure 10 traits describing the response of g_s to a decrease in photosynthetic photon flux density (*PPFD*) in over 2000 plants of 659 accessions in a sorghum association mapping population. Results were validated against photosynthetic gas-exchange measurements. Phenotypic trait correlations were used to identify general patterns in stomatal behavior. GWAS and TWAS were performed to identify phenotype to genotype associations, along with an ensemble approach combining GWAS and TWAS results using the Fisher's combined test (FCT) (Kremling et al., 2019), followed by a GO enrichment analysis. The resulting list of 239 candidate genes identified with greatest confidence was enriched in orthologs of genes implicated in stomatal and photosynthetic traits in Arabidopsis and maize.

162

Results

The response of g_s estimated from thermal imaging ($g_{s\ thermal}$) to a reduction in *PPFD* from 750 to 75 µmol m^{-2} s^{-1} was measured in 659 sorghum accessions (Table 1; Fig. 1). On a subset of 64 plants, g_s estimates were also obtained from gas-exchange measurements to validate $g_{s\ thermal}$ as a proxy for g_s. Both $g_{s\ thermal}$ and g_s predicted a similar pattern of stomatal closure upon a decrease in *PPFD*, sometimes followed by re-opening at low *PPFD* (Fig. 2). All traits derived from $g_{s\ thermal}$ were significantly and positively correlated with their equivalents from g_s (p<0.005, Pearson's r ranging from 0.38 - 0.59, Spearman's rank-order ρ ranging from 0.29 - 0.66, Fig. 3).

Genetic variation, heritability, and trait correlations

Variation among accessions was 3-fold, 10-fold, 6-fold, and 8-fold, respectively, for steady-state $g_{s\ thermal}$ at high *PPFD* ($g_{s\ light}$), steady-state $g_{s\ thermal}$ at low *PPFD* ($g_{s\ shade}$), the amplitude of decline in $g_{s\ thermal}$ from high to low *PPFD* ($g_{s\ light}$ - $g_{s\ shade}$), and integrated $g_{s\ thermal}$ throughout the low-*PPFD* period ($g_{s\ \Sigma\ shade}$, Table 1). For example, $g_{s\ light}$ in accession PI552851 was more than double that of accession PI267653 (Fig. 4A-B). After the decrease in *PPFD*, $g_{s\ thermal}$ declined at an exponential rate ($V_{initial}$), then reached a minimum ($g_{s\ initial\ min}$), and the time to reach this minimum was recorded ($t_{initial\ min}$). Variation among accessions was 28-fold, 9-fold, and 7-fold, respectively, for $V_{initial}$, $g_{s\ initial\ min}$, and $t_{initial\ min}$, respectively (Table 1). For example, the decline of $g_{s\ thermal}$ was faster in PI267653, which displayed a strongly negative $V_{initial}$ and low $t_{initial\ min}$ relative to slower accessions such as PI552851 (Fig. 4A-B). Stomatal re-opening often occurred after the initial decline causing a dampened oscillation in $g_{s\ thermal}$ during adjustment to low *PPFD*. The variation among accessions was 37-fold, 7-fold, and 9-fold, respectively, for the linear increase in $g_{s\ thermal}$ ($V_{oscillation}$), $g_{s\ thermal}$ at peak stomatal re-opening ($g_{s\ oscillation\ max}$) and the amplitude of oscillation ($g_{s\ oscillation\ max}$ - $g_{s\ initial\ min}$). For example, the oscillation of $g_{s\ thermal}$ was more pronounced in NSL50717, which displayed high $V_{oscillation}$ and high oscillation amplitude ($g_{s\ oscillation\ max}$ - $g_{s\ initial\ min}$), relative to PI660605, which showed no stomatal re-opening (Fig. 4C-D). Oscillation of $g_{s\ thermal}$ occurred on different timescales, e.g. more protracted in PI329646 than PI660630 (Fig. 4E-F). Variation in these traits among genotypes was reproducible across replicates (Fig. 4A-F).

Genomic heritability (h^2) was highest (0.67-0.72) in traits describing $g_{s\ thermal}$ at low *PPFD*, including $g_{s\ initial\ min}$, $g_{s\ oscillation\ max}$, $g_{s\ shade}$, and $g_{s\ \Sigma\ shade}$ (Table 1). Traits describing the speed of change in $g_{s\ thermal}$ after a decrease in *PPFD* ($V_{initial}$, $t_{initial\ min}$) also had moderately high h^2 (0.67-0.68). Traits describing the oscillation in $g_{s\ thermal}$ during stomatal re-opening at low *PPFD* ($V_{oscillation}$, $g_{s\ oscillation\ max}$ - $g_{s\ initial\ min}$) had low to intermediate h^2 (0.24-0.49). h^2 was low (0.31) in traits describing $g_{s\ thermal}$ at high *PPFD* and the amplitude of overall decline in $g_{s\ thermal}$ from high to low *PPFD*: $g_{s\ light}$ and $g_{s\ light}$ - $g_{s\ shade}$, respectively.

All traits were correlated (r from -0.29 – 0.94) with one another (p<0.05, Fig. 5, Supplementary Fig. S1). In particular, accessions with high $g_{s\ thermal}$ at high *PPFD* also had greater overall $g_{s\ thermal}$ at low *PPFD* (positive correlation of $g_{s\ light}$ and $g_{s\ \Sigma\ shade}$, p<0.0001, r=0.58, Fig. 6A), took longer to adjust to the decrease in *PPFD* (positive correlation of $g_{s\ light}$ and $t_{initial\ min}$, p<0.0001, r=0.3; positive correlation of $g_{s\ light}$ and $V_{initial}$, p<0.0001, r=0.34, Fig. 6B-C), and had more pronounced stomatal re-opening at low *PPFD* (positive correlation of $g_{s\ light}$ and $V_{oscillation}$, p<0.0001, r=0.21, Fig. 6D).

GWAS, TWAS, FCT and GO enrichment analysis

For each $g_{s\ thermal}$ trait, genes were initially identified as of potential interest if they were in linkage disequilibrium (LD) (Supplementary Table S1) with the top 0.1% strongest associated SNPs from GWAS (~600 genes per trait; Supplementary Table S2); among the top 1% strongest associated genes from TWAS for leaf or shoot tissues (199 and 169 genes per trait, respectively; Supplementary Table S3); or among the top 1% strongest associated genes from FCT for leaf or shoot tissues (150 genes per trait; Supplementary Table S4). In addition to individual traits, multi-trait associations were performed with two trait groups: G1) traits describing the speed of change in $g_{s\ thermal}$ after a decrease in *PPFD* ($V_{initial}$, $t_{initial\ min}$), and G2) traits describing overall values of $g_{s\ thermal}$ ($g_{s\ light}$, $g_{s\ initial\ min}$, $g_{s\ oscillation\ max}$, $g_{s\ shade}$, $g_{s\ \Sigma\ shade}$). The compilation of these results (Table S5) indicated that there was significant overlap in genes identified for different $g_{s\ thermal}$ traits, with 37% of genes being identified for two or more traits (Table 2).

Follow-up analyses were also performed to identify a subset of "higher confidence" genes, i.e. genes for which there was evidence for an association of trait variation with DNA sequence variation (GWAS) and RNA transcript abundance (TWAS), or genes identified in tests

from both of the two independent approaches to sampling developing leaf tissue i.e. from the 3rd *leaf* or *shoot* section containing the growing point. Therefore, genes overlapping the top hits for multiple analyses/tissues, i.e. GWAS, TWAS leaf, TWAS shoot, FCT leaf, and/or FCT shoot (n. overlaps ≥2 in Supplementary Table S5), were further investigated (Supplementary Fig. S2-S12). Across all traits, 1548 candidate genes were identified consistently across two or more of the individual tests. Taking $V_{initial}$ as a representative trait, of the 1007 top hits, 180 were identified from at least two analyses/tissues (Fig. 7).

GO enrichment analysis on Arabidopsis orthologs of the "higher confidence" genes identified 153 significantly enriched biological processes (FDR-adjusted $p<0.05$), nested within 34 broad categories (Supplementary Table S6). Among these, 22 categories of biological processes (e.g. *regulation of histone H3-K27 methylation*, *hydrogen peroxide metabolic process*, *cell cycle DNA replication*, *plant epidermis morphogenesis*, *lipid catabolic process* and *plant-type cell wall biogenesis*) were enriched by >2.5-fold (Fig. 8). A total of 239 unique genes contained within these GO categories were considered the strongest candidates to underlie variation in stomatal conductance traits studied here. A survey of the literature on their orthologs in Arabidopsis, maize and rice revealed a large proportion of genes (32 %) had functions related to stomatal opening/closing (24 genes), stomatal/epidermal cell development (35 genes), leaf/vasculature development (12 genes), or chlorophyll metabolism/photosynthesis (8 genes) (Supplementary Table S7).

241

Discussion

Stomatal responses to changes in *PPFD* influence WUE of plants in fluctuating light environments (Lawson and Blatt, 2014). This study successfully met the objectives of: (1) demonstrating how high-throughput thermal imaging can be used to rapidly phenotype variation in stomatal closure responses to PPFD across a diverse population of C_4 plants; and (2) using that HTP data to perform an integrated GWAS/TWAS that identified a compelling set of candidate genes for further investigation of stomatal opening and closing in C_4 species. Thermal measurements were validated against classical gas-exchange, and phenotypic correlations revealed relationships between steady-state (e.g. $g_{s\ light}$) and dynamic (e.g. $V_{initial}$) stomatal conductance traits. Results showed substantial, heritable variation in dynamic responses of stomata to a reduction in *PPFD*. This study presents important new information on sorghum, a model system with rapid stomatal movement compared to other species (McAusland et al., 2016), and addresses a major knowledge gap that exists for C_4 species, despite their agricultural and ecological importance (Edwards et al., 2010; Leakey et al., 2019).

Validation of $g_{s\ thermal}$ as a high-throughput proxy for g_s

Although dynamic g_s responses have been increasingly studied in the past few years (McAusland et al., 2016; Deans et al., 2019; Acevedo-Siaca et al., 2020; De Souza et al., 2020; Pignon et al., 2021), measurements have not yet been deployed at a scale amenable to association mapping (e.g., GWAS). Here, $g_{s\ thermal}$ was a useful high-throughput proxy for g_s, enabling simultaneous measurement of 18 plants in a single imaging frame. Previous studies have reported near-perfect correlation between $g_{s\ thermal}$ and g_s when it was examined globally across an entire dataset i.e. where g_s varied by more than an order of magnitude as a result of combining data from multiple PPFDs, species and genotypes (Spearman's rank-order ρ=0.96) (McAusland et al., 2013). In contrast, the present study focused on testing the correlations between estimates of individual traits measured by photosynthetic gas exchange versus thermal imaging at higher throughput. For example, thermal imaging was highly significant ($p<0.001$) in capturing variation in g_s measured by gas exchange at a single PPFD (ρ ranging from 0.29 - 0.66, Fig. 3) and this thermal estimate of $g_{s\ shade}$ had a heritability of 0.70, making it suitable for association mapping. It is also notable that correlations between the two measurement approaches would have been weakened because $g_{s\ thermal}$ and g_s were not measured simultaneously in the manner

that McAusland et al. (2013) achieved so elegantly. For example, consistency between the two approaches to g_s measurements was likely reduced by differences in measurement conditions and the immediate history of environmental conditions experienced by leaves as they moved from thermal measurements to the gas exchange chamber. Boundary layer conductance was likely lower while measuring $g_{s\ thermal}$ than g_s due to the air mixing fan used in gas-exchange equipment (Grant et al., 2006). Light quality was equal parts red/blue/green for $g_{s\ thermal}$ vs. 90% red 10% blue for g_s. This likely affected stomatal opening, which is induced by blue, and to a lesser extent, red light (Assmann and Shimazaki, 1999; Shimazaki et al., 2007; Lawson et al., 2011; Assmann and Jegla, 2016). For these reasons, the significant correlations between all traits estimated from $g_{s\ thermal}$ and their counterparts estimated from gas exchange measurements were considered a validation of the methods used.

Sorghum shows varied, heritable stomatal responses to a decrease in *PPFD*

Within-species diversity in stomatal light responses has been documented for C_3 species including Arabidopsis (Takahashi et al., 2015), poplar (Durand et al., 2019), rice (Acevedo-Siaca et al., 2020), cassava (De Souza et al., 2020) and soybean (Soleh et al., 2016). Expanding the scale of investigation to 659 accessions of sorghum revealed substantial variation within the C_4 model species, despite the fact that C_4 species generally have lower g_s than C_3 species (Taylor et al., 2010). The range of $t_{initial\ min}$ shown here (1.8-13.4 minutes, Table 1) overlapped with similar measurements in sorghum (~2-8 minutes) (McAusland et al., 2016; Pignon et al., 2021), the closely related C_4 grasses miscanthus and maize (~8 minutes), the C_3 grass rice (~10 minutes) (McAusland et al., 2016), and the semi-aquatic rhizomatous fern *Marsilea drummondii* A. Braun (~9 minutes) (Deans et al., 2019). Some C_3 dicots such as Arabidopsis and sunflower (~18 minutes) were roughly comparable to the slowest accession shown here ($t_{initial\ min}$ =13.4 minutes), while many other species appeared considerably slower (~30 minutes) (McAusland et al., 2016; Deans et al., 2019). The faster stomata of sorghum might be related to the unique structure of graminaceous stomata, composed of dumbbell-shaped guard cells flanked by subsidiary cells, which have been linked to rapid movement relative to other forms (Franks and Farquhar, 2007; Lawson et al., 2011; Serna, 2011; McAusland et al., 2016; Lawson and Vialet-Chabrand, 2019). Stomata of C_4 plants tend to be smaller and more sensitive to environmental change than their C_3 counterparts (Lawson et al., 2011; McAusland et al., 2016).

Implications of natural diversity in stomatal responses to decreasing *PPFD*

Compared to steady-state g_s under high *PPFD,* traits describing the dynamic change in $g_{s\ thermal}$ after a decrease in *PPFD* had greater variability and h^2, making them more tractable targets for association studies (Table 1). Additionally, variation in traits describing the speed of change in $g_{s\ thermal}$ after a decrease in *PPFD* ($V_{initial}$, $t_{initial\ min}$) might be leveraged to accelerate stomatal responses even in species with "fast" stomata such as sorghum, potentially improving coordination of g_s with photosynthetic carbon assimilation (A) and resulting in improved *iWUE* (Lawson and Blatt, 2014).

The relationships among traits observed across the genetic variation surveyed here are consistent with biophysical trade-offs driven by structure-functional relationships, as well as selection for trait combinations that favor carbon gain versus water savings to differing degrees in different environments. For example, the finding that accessions with greater $g_{s\ light}$ took longer to adjust to a decrease in *PPFD* (Fig. 6B-C) is consistent with greater $g_{s\ light}$ being associated with larger stomata and longer times for pores to close in a subset of the lines studied here (Pignon et al., 2021) and in tests of diverse species (McAusland et al., 2016). However, it is worth noting that variation in stomatal opening/closing is also associated with guard cell physiology, including ion transport processes (Lawson and Blatt 2014). Adaptation to different environments may also contribute to the observed trait correlations, with high $g_{s\ light}$ and slow stomatal closure working in concert to favor A and rapid growth in environments where water is not limiting. In contrast, low $g_{s\ light}$ and rapid stomatal closure combine to prioritize water-use efficiency and conservative but sustained growth in water-limited environments (Vico et al., 2011). Since more rapid stomatal closure after a decrease in PPFD would increase iWUE, there is significant interest in identifying more genes underpinning structural and functional components of stomatal movements, as well as their interactions with steady-state gas exchange and leaf development and physiology more broadly (Lawson and Blatt 2014).

GWAS/TWAS identifies genes enriched in stomatal, leaf developmental and photosynthetic functions

Gene candidates putatively associated with genetic variation in stomatal closure in sorghum were identified using GWAS and TWAS integrated with FCT, followed by GO enrichment analysis. This approach has identified known causal variants more efficiently than

GWAS and TWAS alone (Kremling et al. 2019), while also increasing the consistency in results observed when testing was repeated across different conditions (Ferguson et al. 2020). The present study reinforced these prior reports, with an order of magnitude more genes being consistently identified by FCT versus TWAS across the two independent tissue sampling strategies used (Table S5). GO enrichment analysis of the Arabidopsis orthologues of these genes revealed 22 GO biological processes that were significantly and >2.5-fold enriched (Supplementary Table S6, Fig. 8). The 239 genes belonging to these 22 categories were selected as the greatest confidence candidate genes (Fig. 8; Supplementary Table S7). A large proportion (32%) of these genes have orthologs in Arabidopsis, maize or rice that are already implicated in regulating traits related to stomata or WUE. While it is unlikely that such enrichment would occur by random chance, the function of the genes identified here will require confirmation by follow-up reverse genetic studies of transgenic or mutant plants.

Twenty three orthologs of genes implicated in signaling, metabolism or transporters in guard cells belong to enriched GO terms including *lipid catabolic process*, *hydrogen peroxide metabolic process*, *response to disaccharide* and *response to heat* (Supplementary Table S7). For example, loss of ascorbate peroxidase 1 (APX1) and the Respiratory burst oxidase homolog protein F (RBOHF) influence redox oxygen species (ROS) to alter stomatal responses to light, [CO_2] or abscisic acid (ABA; Pnueli et al., 2003; Chater et al., 2015; Sierla et al., 2016). Meanwhile, the MYB60 transcription factor is required for light induced opening of stomata in Arabidopsis. It is expressed exclusively in guard cells, with expression increasing and decreasing in accordance with conditions that promote stomatal opening and closing, respectively (Cominelli et al., 2005). Phospholipase Dα1 (PLDα1) and its lipid product phosphatidic acid impact ABA-induction of ROS production and stomatal closure (Zhang et al., 2009). Mutants of ABC transporter G family member 40 (ABCG40) shut more slowly in response to ABA (Kang et al. 2010), while its sorghum ortholog was variously associated with 5 different g_s thermal traits in GWAS, TWAS and FCT tests.

Recently, lipid metabolism of guard cells was discovered to be important as an energy source for light-induced stomatal opening (McLachlan et al., 2016). Five sorghum genes associated with variation in $g_{s\ thermal}$ traits were orthologs of genes involved in triacyl glyceride mobilization and expressed in guard cells of Arabidopsis (Enoyl-CoA delta isomerase 1 and 3,

362 ECI1 and ECI3; peroxisomal fatty acid beta-oxidation multifunctional protein, MFP2; Acyl-
363 coenzyme A oxidase 2 and 4, ACX2 and ACX4; McLachlan et al., 2016). Notably, Wrinkled1, a
364 transcription factor that regulates metabolic genes in a manner that promotes carbon allocation to
365 fatty acid synthesis, was also identified (Cernac and Benning 2004). Therefore, a significant
366 proportion of the highest confidence candidate genes identified by the integrated GWAS/TWAS
367 are plausibly involved in signaling, metabolism and transport functions in guard cells. Further
368 study will be needed to determine if the candidate genes identified here play specific roles in
369 stomatal closure, or if the associations observed in this study are partly a product of the strong
370 correlations between rates of stomatal opening and closing (Lawson and Blatt 2014). Current
371 understanding of lipid metabolism guard cells would seem to suggest the latter option is more
372 likely, but this area of study is still relatively nascent.

373 The functions of orthologs of the highest confidence sorghum candidate genes are also
374 consistent with the importance of structure-function relationships to the speed of stomatal
375 opening and closing. Thirty five orthologs of genes implicated in stomatal or epidermal cell
376 patterning belong to enriched GO terms including *plant epidermis morphogenesis*, *cell cycle*
377 *DNA replication*, *plant-type cell wall biogenesis*, and *plastid organization* (Supplementary Table
378 S7). Arabidopsis genes known to impact stomatal development or patterning which had sorghum
379 orthologs found in the highest confidence candidates for $g_{s\ thermal}$ traits included: the Mitogen-
380 activated protein kinase kinase kinase YODA (Bergmann et al., 2004), the FAMA bHLH-type
381 transcription factor (Ohashi-Ito and Bergmann 2006), the cyclin-dependent kinase CDKB1;1
382 (Boudolf et al., 2004), the phytochrome interacting factor 1 (PIF1, Klermund et al., 2016),
383 somatic embryogenic receptor kinase 1 (SERK1, Meng et al. 2015), DNA-directed RNA
384 polymerase II subunit 2 (Chen et al., 2016), the chromatin regulator Enhanced Downy Mildew 2
385 (EDM2, Wang et al ., 2016), Protein Phosphatase 2A (Bian et al., 2020), GATA, NITRATE-
386 INDUCIBLE, CARBON METABOLISM-INVOLVED (GNC, Klermund et al., 2016), the extra-
387 large GTP-binding protein (XLG3, Chakravorty et al., 2015), and the ARF guanine-nucleotide
388 exchange factor GNOM (Le et al., 2014). Focusing on grasses, SOBIC.010G277300 shares 96 %
389 predicted protein sequence homology with GRMZM2G057000 in maize. The *nana plant2* (na2)
390 mutant of this gene displays alterations in brassinosteroid synthesis and the morphology of
391 stomatal complexes (Best et al., 2016). Similarly, SOBIC.004G116400 shares 74 % predicted

protein sequence homology with Os02g15950 (ERECT PANICLE 3, EP3) in rice. Loss of function mutants of EP3 have smaller stomata, which appeared to drive reductions in g_s and A (Yu et al., 2015). Given the substantial evidence for links between gas exchange, stomatal complex size and stomatal density (Lawson and Blatt 2014; Xie et al., 2020), there is potential for variations in the sequence and expression of these genes to drive variation in the $g_{s\ thermal}$ traits measured in this study. A number of other genes identified by the integrated GWAS/TWAS have been implicated in the development of epidermal cells in general (Supplementary Table S7). Cross talk between development pathways for stomata and other types of epidermal cells (Kim and Dolan 2011, Raissig et al., 2016) creates the opportunity for such genes to influence g_s and its response to PPFD.

Finally, a smaller number of sorghum genes identified in this study have orthologs known to influence overall leaf development/vasculature (9 genes) or chlorophyll/photosynthesis (7 genes) (Supplementary Table S7). Leaf vasculature determines the hydraulic capacity of the leaf to deliver water that eventually diffuses out of the leaf as vapor. Consequently, strong traits associations between leaf hydraulics and stomata have been described in a range of contexts (Sack et al., 2003; Bartlett et al., 2016). In that vein, it is plausible that genes known to alter vascular development via effects on polyamine metabolism (5'-methylthioadenosine nucleosidase, MTN1, Waduwara-Jayabahu et al., 2012), glucuronoxylan synthesis (Beta-1,4-xylosyltransferase, IRX9, Pena et al., 2007) and transcriptional regulation (DEFECTIVELY ORGANIZED TRIBUTARIES 5, DOT5, Petricka et al., 2008) might be associated with variation in g_s thermal traits. Similarly, identification of genes involved in photosynthesis may reflect the tight linkage between A and g_s, which is observed in many plant species and is particularly strong in sorghum (Leakey et al., 2019). QTL for traits related to A and g_s often overlap, including in sorghum (Ortiz et al., 2017). When compared to other species, sorghum shows exceptional coordination between g_s and A following decreases in *PPFD*, driven by rapid responses in g_s (McAusland et al., 2016). Among diverse sorghum accessions, there is significant covariation between the responses of A and g_s following decreases in *PPFD*, i.e. accessions with more rapid declines in A also have more rapid declines in g_s, and vice-versa (Pignon et al. 2021). Most notable was the identification of the sorghum Rubisco Activase (RCA) by GWAS, TWAS and FCT across 8 different $g_{s\ thermal}$ traits (Supplementary Table S7). RCA encodes an enzyme

that plays a key role in activating Rubisco to perform the key step in photosynthetic CO_2 assimilation (Portis 2003), and which is known to limit the rate of photosynthetic induction after an increase in PPFD (Pearcy 1990). Along with a number of the results described above, this opens the possibility that phenotyping only stomatal closure may have facilitated identification of associations between genotype or gene expression and both stomatal opening and closing, as a result of the two aspects of stomatal movement being so tightly linked. If functional validation of candidate genes supports that notion, then considerable time can be saved when collecting phenotypic data.

Conclusion

This study demonstrates how high-throughput phenotyping by thermal imaging can be used to assess genetic variation in stomatal closure after a decrease in PPFD at a scale suitable for association mapping. Integrated GWAS/TWAS and FCT was then applied to identify a set of candidate genes, which were enriched in orthologs of Arabidopsis, maize and rice genes involved in stomatal opening/closing, epidermal patterning, leaf development and photosynthesis. This is important proof of concept for methods to break the phenotyping bottleneck for a trait that is important to plant productivity and sustainability but has until now been intractable as a target for study by quantitative genetics. The method described here could also be applied to other species from a variety of plant functional types or grown in different environments to assess G×E of stomatal traits. In addition, the study provides new knowledge of trait variation and underlying candidate genes in an important C_4 model crop, which is notable for the speed of its stomatal opening/closing. This lays the foundation for future studies to establish gene function and potentially improve crop performance.

Materials and methods

Physiology measurements

Plant material and growing conditions

A random subset of 659 accessions was selected from the biomass sorghum diversity panel at the University of Illinois at Urbana-Champaign, as previously described (Valluru et al., 2019). Accession names are provided in Supplementary Table S8. Plants were grown from seed in flats (3x6 sets of 281 mL inserts) containing a peat/bark/perlite-based growing medium (Metro-Mix 900; Sun Gro Horticulture, Agawam, MA, USA) and supplemented with 1 mL slow release 13-13-13 fertilizer (Osmocote Classic, Everris NA, Inc., Dublin, OH, USA). One accession, PI147837, was included in each flat to identify spatial and temporal variation in measurements. Three seeds/insert were planted, then thinned to 1 seedling/insert. Flats were watered regularly to field capacity and grown in a greenhouse maintained at 27 °C day/25 °C night, with supplemental lighting to ensure minimum light intensity of 90 W m^{-2} during a 13 h day. n=3-4 plants were assessed per accession.

Experimental conditions and leaf temperature measurement

Once the fourth leaf had fully expanded, as evidenced by ligule emergence, plants were transferred to a growth cabinet overnight (Model PCG20, Conviron, Winnipeg, MB R3H 0R9, Canada). Cabinets were maintained at 14 h/10 h day/night cycle under 1200 µmol photons m^{-2} s^{-1} PAR, 30 °C daytime/25 °C nighttime temperature, and 75% RH. On the day of measurement, the fourth leaf of each plant was laid flat across a frame to standardize leaf angle and incident light interception (Supplementary Fig. S13). This presented a 4 cm length of the mid-leaf for measurement. Leaves were not detached from plants. Dry and wet reference materials were prepared as in McAusland et al. (2013) to correct for the effects of net isothermal radiation and VPD, respectively (Guilioni et al., 2008). A thin coating of petroleum jelly was applied over 1 cm of abaxial and adaxial sides of leaves, providing a dry reference unique to each leaf. Two sections of filter paper, moistened by a water reservoir, were used as a wet reference.

Flats of 18 plants were transferred to a second growth cabinet with conditions identical to the first cabinet, except that light was provided by a 20 x 20 cm LED panel providing equal-parts blue, red and green light, with a combined incident photon flux of 750 µmol m^{-2} s^{-1} at the leaf

level (LED Light Source SL 3500, Photon Systems Instruments, Brno, Czech Republic). An infrared camera (Thermo Gear Model G100, Nippon Avionics CO., Ltd., Tokyo, Japan) was placed 0.5 m above the leaves without obstructing the light source. Incident photon flux was maintained at 750 µmol m^{-2} s^{-1} for 40 minutes, and then reduced by 90% for an additional 60 minutes. Images were recorded every 6 seconds, with emissivity=0.95 (Jones et al., 2002). The cabinet's PAR sensor was used to evaluate spatial heterogeneity of incident photon flux, which was contained to ± 6% variation across the measured area.

Image analysis and stomatal conductance estimation

Analysis of thermal images was performed in ImageJ (ImageJ1.51j8, NIH, USA). Sections of leaf and reference materials of each image were hand-selected to derive profiles of temperature vs. experimental time. Leaf and reference temperatures were used to calculate $g_{s\ thermal}$:

$$g_{s\ thermal} = (T_{dry} - T_{leaf})/(T_{leaf} - T_{wet}) \quad (1)$$

where T_{leaf}, T_{dry}, and T_{wet} are temperatures of the leaf, dry and wet references, respectively. $g_{s\ thermal}$ is theoretically proportional to g_s given constant environmental conditions (Jones, 1999; Jones et al., 2002; Grant et al., 2006; Guilioni et al., 2008; McAusland et al., 2013). Air RH and temperature were controlled by the growth cabinet and assumed constant across all leaf and reference surfaces. Since the cabinet was designed to deliver a uniform airflow, and replicate plantings were randomly positioned to avoid systematic spatial variation, boundary layer conductance was also assumed constant. Differences in $g_{s\ thermal}$ between leaves and over time were therefore attributed to g_s.

Analysis of $g_{s\ thermal}$ profiles

Several traits were derived from profiles of $g_{s\ thermal}$ vs. experimental time: $g_{s\ light}$, $g_{s\ shade}$, $g_{s\ \Sigma\ shade}$, $g_{s\ initial\ min}$, $g_{s\ oscillation\ max}$, $t_{initial\ min}$, $V_{initial}$, and $V_{oscillation}$. A graphical description of these traits is given in Fig. 1. After the decrease in *PPFD*, $g_{s\ thermal}$ declined as stomata closed, often followed by an oscillation in $g_{s\ thermal}$ as stomata re-opened and then closed again. $g_{s\ light}$ and $g_{s\ shade}$ were the average of $g_{s\ thermal}$ from t=-5 to 0, and from t=52 to 60 minutes, respectively. These gave steady-state $g_{s\ thermal}$ at *PPFD* of 750 and 75 µmol m^{-2} s^{-1}, respectively. $g_{s\ \Sigma\ shade}$ was the area beneath the curve following the *PPFD* change, i.e. from t=0 to 60 minutes. $g_{s\ initial\ min}$ was the

minimum of $g_{s\ thermal}$ reached immediately after the decrease in *PPFD*. $g_{s\ oscillation\ max}$ was the maximum of $g_{s\ thermal}$ reached during the stomatal re-opening phase. The time at which $g_{s\ thermal}$ reached 110% of $g_{s\ initial\ min}$ was recorded as $t_{initial\ min}$. The amplitude of the overall change in $g_{s\ thermal}$ from high to low *PPFD* was ($g_{s\ light}$ - $g_{s\ shade}$), and the amplitude of oscillation in $g_{s\ thermal}$ at low *PPFD* was ($g_{s\ oscillation\ max}$ - $g_{s\ initial\ min}$).

$V_{initial}$ was derived from non-linear regression (PROC NLIN, SAS v9.4; SAS Institute, Cary, NC, USA) as the exponential rate of decline of $g_{s\ thermal}$ from t= -0.1 minutes to t= $t_{initial\ min}$:

$$g_{s\ thermal} = a + b * e^{(V_{initial} * \mathrm{time})} \quad (2)$$

here *b* and *a* give estimates of $g_{s\ thermal}$ at t= -0.1 minutes and t=$t_{initial\ min}$, respectively, and a more negative $V_{initial}$ indicates a more rapid decline in $g_{s\ thermal}$. $V_{oscillation}$ was derived from linear regression (PROC GLM, SAS v9.4) as the linear slope of $g_{s\ thermal}$ vs. time during stomatal re-opening at low *PPFD*. A more positive $V_{oscillation}$ indicates a more rapid stomatal re-opening.

Validation of $g_{s\ thermal}$ with gas-exchange measurements

Validation of $g_{s\ thermal}$ as a proxy for g_s was obtained on a subset of 64 plants. After $g_{s\ thermal}$ measurements were completed, plants were placed back in the first growth cabinet. The leaf section previously used for $g_{s\ thermal}$ measurements was placed in the cuvette of a portable gas-exchange system incorporating infra-red CO_2 and water vapor analyzers (LI-COR 6400; LI-COR, Inc., Lincoln, NE USA). Incident *PPFD* was set to 750 µmol m^{-2} s^{-1}, [CO_2] to 400 ppm, and leaf-to-air water vapor pressure deficit maintained <2 kPa. *PPFD* was 10% blue and 90% red light provided by integrated red and blue LEDs. The $g_{s\ thermal}$ measurement protocol was replicated, i.e. initial *PPFD* was maintained for 40 minutes, then reduced by 90% for an additional 60 minutes, with g_s logged every 5 seconds (von Caemmerer and Farquhar, 1981). Pearson's correlation (*r*) at *p*=0.05 threshold, along with Spearman's rank-order correlation (ρ) were tested between equivalent stomatal conductance traits derived from $g_{s\ thermal}$ and g_s using R 3.6.1 (R Core Team, 2017).

When comparing $g_{s\ thermal}$ measurements to this validation data, an anomalous spike in $g_{s\ thermal}$, reaching up to twice the steady-state high-*PPFD* $g_{s\ thermal}$, was consistently recorded from t=0 to 0.9 minutes (Fig. 1). This was likely due to the different radiative properties of the white

wet reference and the green leaf and dry reference. Therefore, $g_{s\ thermal}$ measurements from t=0 to 0.9 minutes were discarded.

Model development for best linear unbiased predictors (BLUPs)

A linear mixed model was used to account for spatial and temporal variation using the ASReml-R package (Butler et al., 2009). The best linear unbiased predictors (BLUPs) were obtained for all accessions and traits and were used for subsequent analysis (Supplementary Table S8). The most appropriate model for each trait was chosen in two steps. First, fixed effects with a Wald statistics *p*-value > 0.05 were excluded from the model. Subsequently, the Akaike information criterion (AIC) was used to select random effects variables and residual variance-covariance structures for each trait. The full model was:

$$y = X\beta + Z_f f + Z_l l + Z_g g + \xi \quad (3)$$

where y is the vector of phenotypes, β is a vector of fixed effects including the intercept, a blocking effect, and a cubic smoothing splines terms for leaf position and time of measurement, with design matrix X. Here the block term refers to three discrete periods throughout the experiment where the LED light had to be repaired and repositioned within the measurement cabinet. The vector f is the vector of random effects of "flat" within block with $f \sim MVN\left(0, \sigma^2_{f/r} I_{f/r}\right)$ and design matrix Z_f. Here the term "flat" refers to a sequential flat number to account for temporal variation between measured flats of plants. The vector l is the vector of random effects of the interaction between row leaf position and column leaf position with $l \sim MVN(0, \sigma^2_l I_l)$ and design matrix Z_l. The vector g is the vector of random genotypic effects of accessions with $g \sim MVN\left(0, \sigma^2_g I_g\right)$ and design matrix Z_g and ξ is the vector of residuals with distribution $\xi \sim MVN\left(0, R \otimes I_{f/r} \oplus I_r\right)$. The matrix $R = \sigma^2_\xi [AR1 \otimes AR1]$ represents the Kronecker product of first-order autoregressive processes across row and column plant positioning within a flat, respectively, and σ^2_ξ is the spatial residual variance. The matrices $I_{f/r}$, I_g, I_l and I_r are the identity matrices of the same dimensions as "flat" within block, genotypic effects, row leaf position and column leaf position interaction effect, and block, respectively. Outliers were removed following method 2 of (Bernal-Vasquez et al., 2016), and the Box-Cox power transformation was used on traits with non-normal residuals.

BLUPs were obtained for all accessions and each trait and added to the grand mean for GWAS and TWAS. Genetic and residual variances estimated from the null GWAS model were used to calculate genomic heritability (h^2) as the ratio of genetic variance over phenotypic variance (de los Campos et al., 2015). Phenotypic correlations between all traits were tested using Pearson's correlation (r) at p=0.05 threshold using cor.mtest() function in package corrplot (Wei and Simko, 2017).

Genomic data collection for GWAS and TWAS

Genotypic data

Genotyping was performed as previously reported (dos Santos et al., 2020). Briefly, DNA from dark-grown etiolated seedling tissue was extracted and placed in 96-well plates following CTAB protocol (Doyle and Doyle, 1987). The genotyping was done using two pairs of restriction enzymes, PstI-HF/HinP1I and PstI-HF/BfaI (New England Biolabs, Ipswich, MA, USA) with the genotyping-by-sequencing (GBS) protocol (Elshire et al., 2011; Morris et al., 2013). Tag alignment was done with Bowtie2 (Langmead and Salzberg, 2012) using the *Sorghum bicolor* genome v3.1 (www.phytozome.jgi.doe.gov). SNPs were identified using the TASSEL3 GBS pipeline (Glaubitz et al., 2014). Reads that did not perfectly match a barcode and restriction site were discarded. After barcode trimming, all unique 64 bp sequences present >9 times in the dataset and that mapped uniquely to the sorghum genome were selected as "master tags." These were compared to tags in each individual at each genomic address to identify SNPs. SNPs with >95% missing data or minor allele frequency (MAF)<5% were discarded.

A HapMap of 239 whole-genome-resequenced sorghum accessions containing 5.5M biallelic phased SNPs with MAF>0.01 (Valluru et al., 2019), was used as a reference panel to impute the GBS data. GBS markers were filtered to only consider markers that were also present in the HapMap. Beagle 4.1 (Browning and Browning, 2016) was used under GT mode with Ne set to 150,000, window=60,000 SNPs, and overlap=4,000 SNPs. After imputation, markers with AR2 < 0.3 were removed, resulting in 2,457,023 SNPs. LD pruning using PLINK (Chang et al., 2015) eliminated markers in high LD (r^2 > 0.9) within 50kb windows. The final dataset consisted of 422,897 SNPs.

Gene expression data

186 sorghum accessions were grown for 3'RNAseq measurement. Environmental conditions were: 12 h/12 h day/night cycle under 500 µmol m^{-2} s^{-1} PAR, 25 °C daytime/23 °C nighttime temperature, and 75% RH. 2 cm of shoot and leaf tissues were sampled at 3rd leaf stage. Samples were processed according to (Kremling et al., 2019). Briefly, RNA was extracted using TRIzol (Invitrogen) with Direct-zol columns (Zymo Research), and 3′ RNA-seq libraries were prepared robotically from 500 ng total RNA in 96-well plates on an NXp liquid handler (Beckman Coulter) using QuantSeq FWD kits (Lexogen) according to the manufacturer's instructions. Libraries were pooled to 96-plex and sequenced with 90 nucleotide single-end reads using Illumina TruSeq primers on an Illumina NextSeq 500 with v2 chemistry at the Cornell University Sequencing facility.

The first 12 bp and Illumina Truseq adapter remnants were removed from each read using Trimmomatic version 0.32, following kit marker instructions. The splice-aware STAR aligner v.2.4.2a was used to align reads against the sorghum v3.1.1 reference genome annotations, allowing a read to map in at most 10 locations (-outFilterMultimapNmax 10) with at most 4% mismatches (–outFilterMismatchNoverLmax 0.04), while filtering out non-canonical intron motifs (–outFilterIntronMotifs RemoveNoncanonicalUnannotated). Default settings from STAR v.2.4.2a aligner were used to obtain gene-level counts (--quantModel GeneCounts) from the resulting BAM files.

GWAS, TWAS and FCT

Traits went through an additional normal quantile transformation, then single and multi-trait associations were performed as in (Zhou and Stephens, 2014). Two groups of multi-trait models were considered: G1) traits describing the speed of change in $g_{s\ thermal}$ after a decrease in *PPFD* ($V_{initial}$, $t_{initial\ min}$), and G2) traits describing overall values of $g_{s\ thermal}$ ($g_{s\ light}$, $g_{s\ initial\ min}$, $g_{s\ oscillation\ max}$, $g_{s\ shade}$, $g_{s\ \Sigma\ shade}$). Both groups of traits went through a step of multivariate outlier removal (Filzmoser et al., 2005) performed before running GWAS and TWAS.

GEMMA (Zhou and Stephens, 2012) was used for single and multivariate GWAS (Zhou and Stephens, 2014). Population structure was accounted for by using principal components (PCs) as fixed effects. Based on the Scree plot, 4 PCs obtained from PLINK (Chang et al., 2015)

using the full SNP dataset (i.e. not LD-pruned) were included in all models. Relatedness was controlled for by a kinship matrix obtained from TASSEL 5 (Bradbury et al., 2007) using the default method (Endelman and Jannink, 2012).

TWAS was tested in developing leaf and shoot tissues with genes expressed in at least half of tested plants. Analyses were implemented in R 3.3.3 (R Core Team, 2017) with the *lm* function used for single-trait TWAS and the MANOVA function for multi-trait TWAS. Similar to (Kremling et al., 2019), 29 Peer factors (Stegle et al., 2010) and five multidimensional scaling factors were used as covariates.

An ensemble approach combining GWAS and TWAS results was performed using the Fisher's combined test (FCT) (Kremling et al., 2019). Briefly, to integrate both the results from GWAS and TWAS, each SNP in the top 10% of GWAS analysis was assigned to the nearest gene. The *p*-values of genes not tested in the TWAS (genes expressed in less than half of tested plants) were set to one. The GWAS and TWAS *p*-values for each gene were combined using Fisher's combined test in *metap* package in R, producing Fisher's combined *p*-values.

Candidate gene analysis

Results of GWAS, TWAS and FCT were used to identify potential candidate genes driving variation in traits. A threshold set at the 0.1% lowest *p*-values was used to identify candidates for each SNP-trait association, i.e., 423 marker associations per trait. This threshold was chosen to focus the analysis on a minimum number of large-effect variants and to limit the number of false positives. PLINK (Chang et al., 2015) was used to calculate LD blocks with option --blocks and a window of 200 kb and default values for D-prime's confidence interval (0.7;0.98) (Supplementary Table S1). Genes within these LD blocks were compiled from the Phytozome database for Sorghum bicolor v3.1.1 (Goodstein et al., 2012). Similarly, the top 1% most strongly associated genes from TWAS and FCT were ascertained for each trait and tissue. Genes were selected for further analysis if they were identified by more than one test of phenotype-genotype associations, i.e. they overlapped the top hit for several analyses/tissues (e.g. overlapping top hits for both GWAS and TWAS leaf). The Arabidopsis orthologs of these genes were collected with INPARANOID (Remm et al., 2001) and used for GO term enrichment analysis in biological function (GO Ontology database DOI: 10.5281/zenodo.4081749 Released

2020-10-09) (Ashburner et al., 2000; Carbon et al., 2019; Mi et al., 2019). PANTHER overrepresentation test was used with Fisher's test and FDR-adjusted *p*-values, with significance declared at $\alpha<0.05$. GO biological processes significantly and >2.5-fold enriched were further considered, and the genes contained within these GO categories were considered the strongest candidates to underlie variation in stomatal conductance traits.

Supplementary material

Supplementary Table S1: LD blocks containing the top 0.1% SNPs from GWAS. The chromosome, upper and lower threshold (bp) for each LD block is also given.

Supplementary Table S2: Top 0.1% strongest GWAS results for each trait, including SNP chromosome and position, marker R^2 and minor allele effect size.

Supplementary Table S3: TWAS results from each tissue and trait, including chromosome position and R^2 for each gene.

Supplementary Table S4: FCT results from each tissue and trait, including the GWAS and TWAS *p*-values taken from Supplementary Tables S2-3 and used to calculate an FCT *p*-value for each gene.

Supplementary Table S5: Summary of genes appearing in the top results for GWAS, TWAS leaf, TWAS shoot, FCT leaf and FCT shoot. An "x" identifies genes present in the top associations for an analysis/tissue. The number of analyses that a gene overlapped the top hits for is also shown, ranging from 1 to 5, where n. overlaps=1 indicates a gene was in the top hits for a single analysis/tissue for a given trait, and n. overlaps=5 indicates a gene was in the top hits for all analyses/tissues for a given trait. The Arabidopsis ortholog of each gene is also given. Arabidopsis orthologs of genes that had n. overlaps of at least 2 were further investigated by GO enrichment analysis (Supplementary Table S6). Genes that were present in a GO enrichment category that was significantly and >2.5-fold enriched are identified.

Supplementary Table S6: GO enrichment analysis of Arabidopsis orthologs of genes overlapping top hits for multiple analyses/tissues. Significantly enriched GO biological processes are shown by hierarchical clustering, with the broadest categories further to the right and categories nested within them listed further to the left. Arrows show hierarchical relationships between GO terms. The n. of known genes in Arabidopsis corresponding to each GO term is given, as well as the observed and expected n. of genes, the fold-enrichment (i.e. ratio of observed to expected genes), and *p*-value used to determine whether the enrichment was statistically significant.

Supplementary Table S7: Summary of the most promising candidate genes, selected because they belong to a GO biological process category significantly enriched by >2.5-fold among the

680 subset of genes overlapping the top results for GWAS, TWAS leaf, TWAS shoot, FCT leaf,
681 and/or FCT shoot. Because GO terms are nested, the broadest GO biological process and its fold-
682 enrichment is presented, along with its nested sub-categories that were also significantly and
683 >2.5-fold enriched. Descriptions for each Arabidopsis gene are given. Genes are identified that
684 were determined by a literature survey to be implicated in a WUE-related trait: the reference
685 used to make this determination is also given. Full references are in supplementary material S1.

686 Supplementary Table S8: BLUPs of all traits for all accessions.

687 Supplementary Table S9: Full GWAS results for each trait.

688

689 Supplementary Material S1: Full reference list from literature review of genes in Supplementary
690 Table S7.

691

692 Supplementary Figure S1: Pearson's correlation coefficients (*r*, top right panels), pairwise
693 correlation scatterplots (bottom left panels) and density plots (diagonal panels) for BLUPs of
694 stomatal traits. Data are the same as in Figure 5.

695 Supplementary Figure S2: GWAS, TWAS and FCT results for $g_{s\ light}$. A: Upset plot showing the
696 number of overlapping genes between the top hits in GWAS, TWAS leaf, TWAS shoot, FCT
697 leaf, and/or FCT shoot. B: Manhattan plots of GWAS, TWAS and FCT results.

698 Supplementary Figure S3: GWAS, TWAS and FCT results for $g_{s\ shade}$. A: Upset plot showing the
699 number of overlapping genes between the top hits in GWAS, TWAS leaf, TWAS shoot, FCT
700 leaf, and/or FCT shoot. B: Manhattan plots of GWAS, TWAS and FCT results.

701 Supplementary Figure S4: GWAS, TWAS and FCT results for $g_{s\ oscillation\ max}$. A: Upset plot
702 showing the number of overlapping genes between the top hits in GWAS, TWAS leaf, TWAS
703 shoot, FCT leaf, and/or FCT shoot. B: Manhattan plots of GWAS, TWAS and FCT results.

Supplementary Figure S5: GWAS, TWAS and FCT results for $g_{s\ initial\ min}$. A: Upset plot showing the number of overlapping genes between the top hits in GWAS, TWAS leaf, TWAS shoot, FCT leaf, and/or FCT shoot. B: Manhattan plots of GWAS, TWAS and FCT results.

Supplementary Figure S6: GWAS, TWAS and FCT results for $g_{s\ \Sigma\ shade}$. A: Upset plot showing the number of overlapping genes between the top hits in GWAS, TWAS leaf, TWAS shoot, FCT leaf, and/or FCT shoot. B: Manhattan plots of GWAS, TWAS and FCT results.

Supplementary Figure S7: GWAS, TWAS and FCT results for $g_{s\ light}$ - $g_{s\ shade}$. A: Upset plot showing the number of overlapping genes between the top hits in GWAS, TWAS leaf, TWAS shoot, FCT leaf, and/or FCT shoot. B: Manhattan plots of GWAS, TWAS and FCT results.

Supplementary Figure S8: GWAS, TWAS and FCT results for $t_{initial\ min}$. A: Upset plot showing the number of overlapping genes between the top hits in GWAS, TWAS leaf, TWAS shoot, FCT leaf, and/or FCT shoot. B: Manhattan plots of GWAS, TWAS and FCT results.

Supplementary Figure S9: GWAS, TWAS and FCT results for $V_{oscillation}$. A: Upset plot showing the number of overlapping genes between the top hits in GWAS, TWAS leaf, TWAS shoot, FCT leaf, and/or FCT shoot. B: Manhattan plots of GWAS, TWAS and FCT results.

Supplementary Figure S10: GWAS, TWAS and FCT results for $g_{s\ oscillation\ max}$ - $g_{s\ oscillation\ min}$. A: Upset plot showing the number of overlapping genes between the top hits in GWAS, TWAS leaf, TWAS shoot, FCT leaf, and/or FCT shoot. B: Manhattan plots of GWAS, TWAS and FCT results.

Supplementary Figure S11: GWAS, TWAS and FCT results for G2. A: Upset plot showing the number of overlapping genes between the top hits in GWAS, TWAS leaf, TWAS shoot, FCT leaf, and/or FCT shoot. B: Manhattan plots of GWAS, TWAS and FCT results.

Supplementary Figure S12: GWAS, TWAS and FCT results for G1. A: Upset plot showing the number of overlapping genes between the top hits in GWAS, TWAS leaf, TWAS shoot, FCT leaf, and/or FCT shoot. B: Manhattan plots of GWAS, TWAS and FCT results.

Supplementary Figure S13: Photograph (right) and corresponding thermal image (left) of experimental setup.

731

732 # Tables

733 Table 1: Descriptive statistics of stomatal conductance traits. h^2 is genomic heritability. $t_{initial\ min}$ is in minutes, all other traits are

734 dimensionless. Graphical description of these traits is given in Fig. 1.

Trait	Description	Mean	SD	Min	Max	h^2
$g_{s\ light}$	Steady-state $g_{s\ thermal}$ at high *PPFD*	0.58	0.08	0.31	0.89	0.31
$g_{s\ shade}$	Steady-state $g_{s\ thermal}$ at low *PPFD*	0.17	0.07	0.05	0.49	0.70
$(g_{s\ light} - g_{s\ shade})$	Amplitude of overall decline in $g_{s\ thermal}$ from high to low *PPFD*	0.41	0.08	0.11	0.66	0.31
$g_{s\ initial\ min}$	Minimum $g_{s\ thermal}$ reached after the *PPFD* decrease	0.05	0.04	-0.03	0.24	0.71
$g_{s\ oscillation\ max}$	Maximum $g_{s\ thermal}$ reached as stomata re-opened at low *PPFD*	0.20	0.07	0.08	0.53	0.67
$(g_{s\ oscillation\ max} - g_{s\ initial\ min})$	Amplitude of oscillation of $g_{s\ thermal}$ at low *PPFD*	0.15	0.05	0.05	0.43	0.49
$t_{initial\ min}$	Time for $g_{s\ thermal}$ to reach 110% of $g_{s\ initial\ min}$	5.2	1.6	1.8	13.4	0.68
$g_{s\ \Sigma\ shade}$	Area beneath the $g_{s\ thermal}$ curve following the *PPFD* decrease	84	32	28	231	0.72
$V_{initial}$	Exponential rate of decline in $g_{s\ thermal}$ after the *PPFD* decrease	-0.89	0.27	-2.23	-0.08	0.67
$V_{oscillation}$	Linear rate of increase in $g_{s\ thermal}$ as stomata re-opened at low *PPFD*	0.0052	0.0028	0.0006	0.022	0.24

735

736

737 Table 2: N. of genes overlapping the top results of GWAS, TWAS and/or FCT in multiple traits.

N. of overlapping traits	N. of genes
1	4575
2	1463
3	689
4	281
5	150
6	97
7	38
8	11
9	6
10	1

738

739

740

741

Figure legends

Figure 1: Schematic of $g_{s\ thermal}$ analysis method, where $g_{s\ thermal}$ is a proxy for stomatal conductance to water vapor (g_s) that is derived from thermal imaging. Each response was measured on a single leaf of sorghum, exposed to *PPFD*=750 µmol m^{-2} s^{-1} for 40 minutes. At t=0, indicated by an arrow, *PPFD* was reduced by 90%. Black circles show $g_{s\ thermal}$. Crosses show measurements from t=0 to t=0.9 minutes which were removed because they consistently showed an anomalous spike. $g_{s\ light}$, the steady-state high-*PPFD* value of $g_{s\ thermal}$, was the mean $g_{s\ thermal}$ from t=-5 to 0 minutes (red circle). $g_{s\ shade}$, the steady-state low-*PPFD* value of $g_{s\ thermal}$, was the mean $g_{s\ thermal}$ from t=52 to 60 minutes (blue circle). $g_{s\ \Sigma\ shade}$ was the area under the curve from t=0 to 60 minutes. $g_{s\ initial\ min}$ was the minimum of $g_{s\ thermal}$ reached immediately after the decrease in *PPFD* (orange circle). $g_{s\ oscillation\ max}$ was the maximum of $g_{s\ thermal}$ reached during stomatal re-opening at low *PPFD* (pink circle). The time at which $g_{s\ thermal}$ reached 110% of $g_{s\ initial\ min}$ was recorded as $t_{\ initial\ min}$ (dotted orange line). $V_{initial}$, the initial rate of decline in $g_{s\ thermal}$ after the decrease in *PPFD*, was the exponential rate of decline of $g_{s\ thermal}$ t=-0.1 minutes to t= $t_{\ initial\ min}$ (solid green line). $V_{oscillation}$ was the linear rate of increase in $g_{s\ thermal}$ during stomatal reopening at low *PPFD* (dashed green line).

Figure 2: Representative responses of $g_{s\ thermal}$ and g_s to a 90% drop in *PPFD* for two accessions: PI455257 and PI525728. $g_{s\ thermal}$ was measured from thermal imaging as a proxy for g_s. Each $g_{s\ thermal}$ response curve was measured on a single leaf, acclimated to *PPFD*=750 µmol m^{-2} s^{-1} for 40 minutes, then *PPFD* was reduced by 90% for 60 minutes at t=0, indicated by an arrow. On a subset of plants, including the two shown here, the protocol was immediately repeated to measure g_s using gas exchange.

Figure 3: Correlation scatterplots between stomatal conductance traits derived from $g_{s\ thermal}$ measurements and their counterparts derived from g_s measurements. Data are for a subset of plants that were first imaged using a thermal camera to obtain $g_{s\ thermal}$, then immediately measured with gas exchange to obtain g_s. $t_{initial\ min}$ is in minutes, all other $g_{s\ thermal}$ traits are dimensionless. Pearson's *r* and the associated *p*-value, along with Spearman's rank-order ρ, are also given.

Figure 4: Representative responses of $g_{s\ thermal}$ to a 90% decrease in *PPFD* in six accessions, selected to highlight the diverse stomatal responses to decreasing *PPFD* measured in the sorghum diversity panel. Different symbols and shades of gray show distinct replicate plants for each accession. Each $g_{s\ thermal}$ response curve was measured on a single leaf, acclimated to *PPFD*=750 µmol m^{-2} s^{-1} for 40 minutes, then *PPFD* was reduced by 90% for 60 minutes at t=0, indicated by an arrow. Values in the table are the mean of stomatal conductance traits for each accession. $t_{initial\ min}$ is in minutes, all other traits are dimensionless.

Figure 5: Pearson's correlation coefficients (*r*) between BLUPs of stomatal conductance traits. The size of circles indicates the strength of correlation, while color indicates whether the pairwise relationship was negative ($r<0$, red) or positive ($r>0$, blue). All corresponding scatterplots are given in Supplementary Fig. S1.

Figure 6: Correlation scatterplots between BLUPs for stomatal conductance traits. Pearson's *r* and the associated *p*-value are also given.

Figure 7: GWAS, TWAS and FCT results for $g_{s\ light}$. A: Upset plot showing the number of overlapping genes between the top hits in GWAS, TWAS leaf, TWAS shoot, FCT leaf, and/or FCT shoot. B: Manhattan plots of GWAS, TWAS and FCT results. Top hits are highlighted if they correspond to orthologues of known Arabidopsis stomatal genes (FMA, POLAR and EPF2, Table 3). Top hits are also highlighted if they are among the highest confidence genes identified by GWAS, TWAS, FCT, and subsequent GO enrichment analysis. (Supplementary Table S7). Equivalent figures for all other traits are in Supplemental Figures S2-12.

Figure 8: Results of GO enrichment analysis of higher confidence genes. Bars gives the number of genes included in each of the categories of GO biological processes that were significantly and >2.5-fold enriched. Fold-enrichment is shown in the label beneath each bar. Full GO enrichment analysis results are in Supplementary Table S6.

781

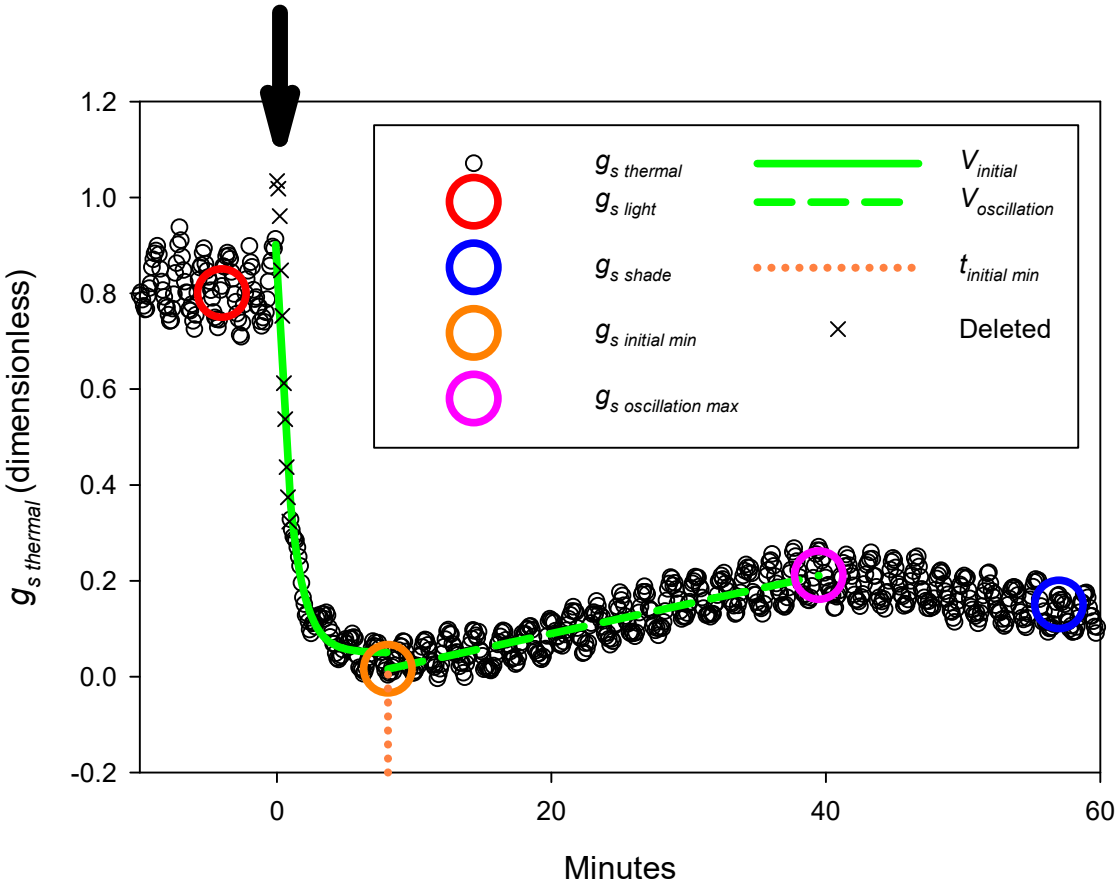

Figure 1: Schematic of $g_{s\ thermal}$ analysis method, where $g_{s\ thermal}$ is a proxy for stomatal conductance to water vapor (g_s) that is derived from thermal imaging. Each response was measured on a single leaf of sorghum, exposed to *PPFD*=750 µmol m^{-2} s^{-1} for 40 minutes. At t=0, indicated by an arrow, *PPFD* was reduced by 90%. Black circles show $g_{s\ thermal}$. Crosses show measurements from t=0 to t=0.9 minutes which were removed because they consistently showed an anomalous spike. $g_{s\ light}$, the steady-state high-*PPFD* value of $g_{s\ thermal}$, was the mean $g_{s\ thermal}$ from t=-5 to 0 minutes (red circle). $g_{s\ shade}$, the steady-state low-*PPFD* value of $g_{s\ thermal}$, was the mean $g_{s\ thermal}$ from t=52 to 60 minutes (blue circle). $g_{s\ \Sigma\ shade}$ was the area under the curve from t=0 to 60 minutes. $g_{s\ initial\ min}$ was the minimum of $g_{s\ thermal}$ reached immediately after the decrease in *PPFD* (orange circle). $g_{s\ oscillation\ max}$ was the maximum of $g_{s\ thermal}$ reached during stomatal re-opening at low *PPFD* (pink circle). The time at which $g_{s\ thermal}$ reached 110% of $g_{s\ initial\ min}$ was recorded as $t_{\ initial\ min}$ (dotted orange line). $V_{initial}$, the initial rate of decline in $g_{s\ thermal}$ after the decrease in *PPFD*, was the exponential rate of decline of $g_{s\ thermal}$ t=-0.1 minutes to t= $t_{\ initial\ min}$ (solid green line). $V_{oscillation}$ was the linear rate of increase in $g_{s\ thermal}$ during stomatal reopening at low *PPFD* (dashed green line).

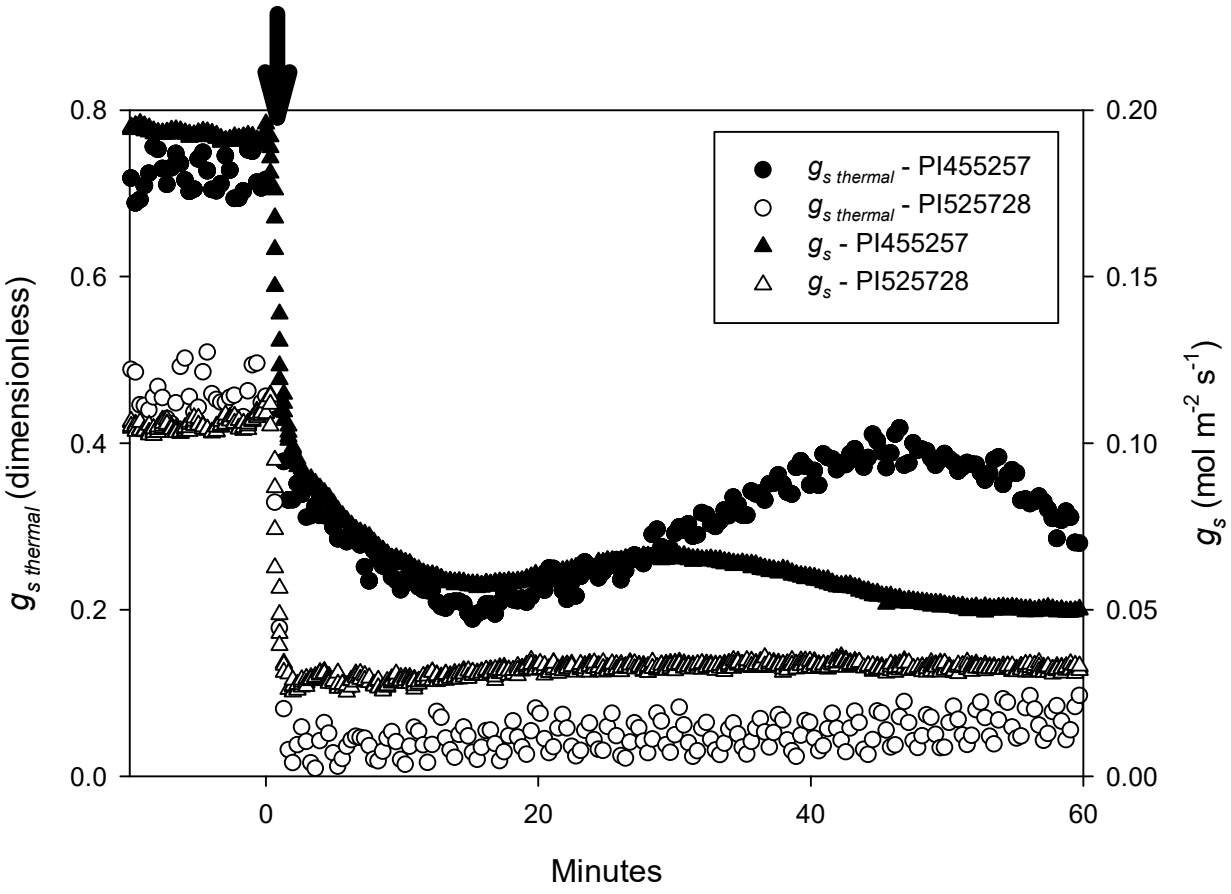

Figure 2: Representative responses of $g_{s\ thermal}$ and g_s to a 90% drop in *PPFD* for two accessions: PI455257 and PI525728. $g_{s\ thermal}$ was measured from thermal imaging as a proxy for g_s. Each $g_{s\ thermal}$ response curve was measured on a single leaf, acclimated to *PPFD*=750 µmol m^{-2} s^{-1} for 40 minutes, then *PPFD* was reduced by 90% for 60 minutes at t=0, indicated by an arrow. On a subset of plants, including the two shown here, the protocol was immediately repeated to measure g_s using gas exchange.

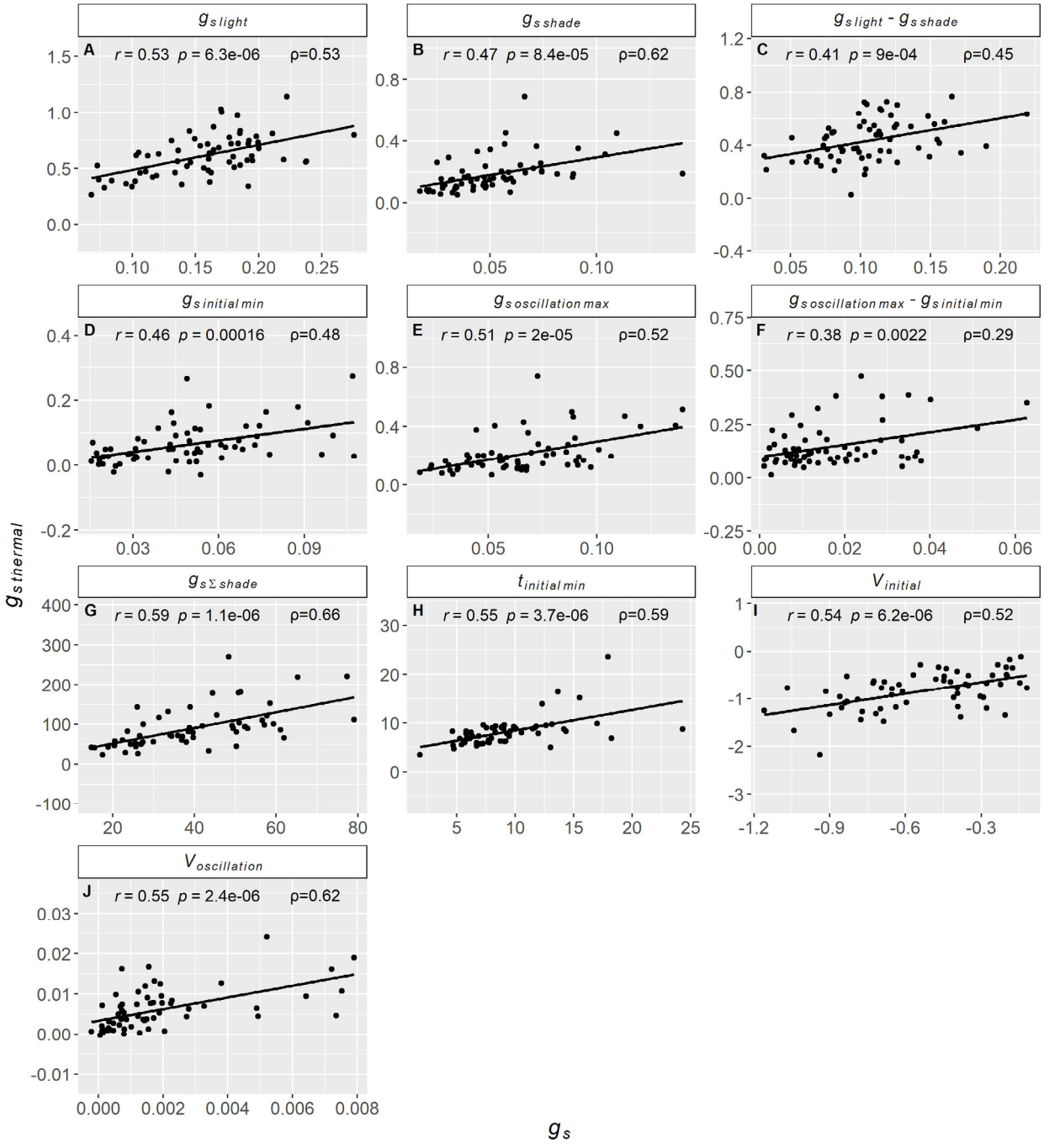

Figure 3: Correlation scatterplots between stomatal conductance traits derived from $g_{s\ thermal}$ measurements and their counterparts derived from g_s measurements. Data are for a subset of plants that were first imaged using a thermal camera to obtain $g_{s\ thermal}$, then immediately measured with gas exchange to obtain g_s. $t_{initial\ min}$ is in minutes, all other $g_{s\ thermal}$ traits are dimensionless. Pearson's r and the associated p-value, along with Spearman's rank-order ρ, are also given.

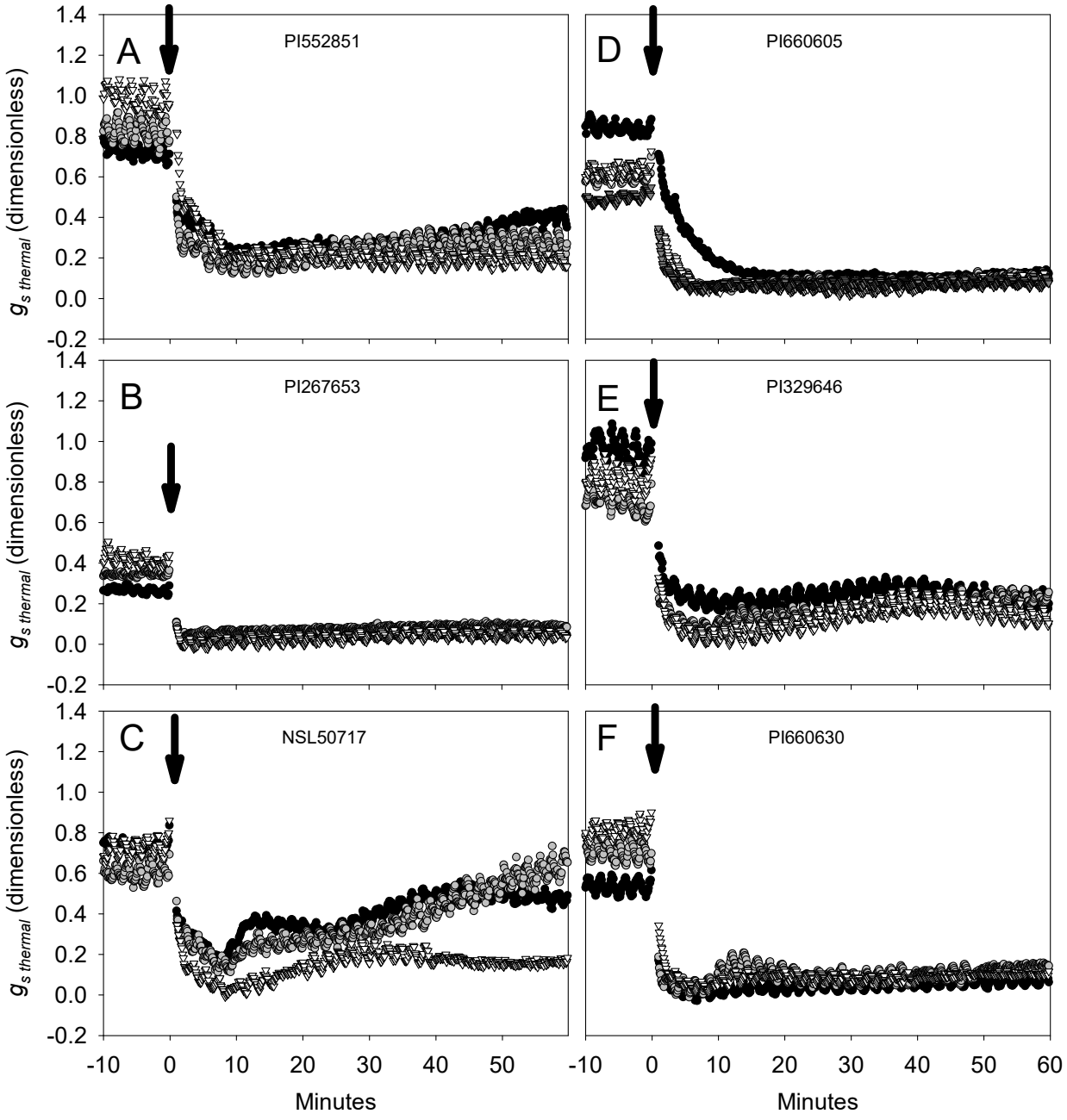

Accession	$g_{s\ light}$	$g_{s\ shade}$	$g_{s\ light} - g_{s\ shade}$	$g_{s\ initial\ min}$	$g_{s\ oscillation\ max}$	$g_{s\ oscillation\ max} - g_{s\ initial\ min}$	$t_{initial\ min}$	$g_{s\ \Sigma\ shade}$	$V_{initial}$	$V_{oscillation}$
NSL50717	0.69	0.42	0.27	0.09	0.32	0.23	5.6	179	-0.76	0.021
PI267653	0.34	0.06	0.28	0.01	0.09	0.08	2.4	30	-1.58	0.001
PI329646	0.81	0.20	0.61	0.07	0.26	0.19	4.9	106	-0.96	0.008
PI552851	0.84	0.29	0.55	0.18	0.36	0.18	7.5	150	-0.41	0.003
PI660605	0.64	0.10	0.54	0.05	0.11	0.06	6.1	58	-0.48	0.003
PI660630	0.69	0.11	0.58	-0.01	0.15	0.16	3.4	47	-1.22	0.010

Figure 4: Representative responses of $g_{s\ thermal}$ to a 90% decrease in *PPFD* in six accessions, selected to highlight the diverse stomatal responses to decreasing *PPFD* measured in the sorghum diversity panel. Different symbols and shades of gray show distinct replicate plants for each accession. Each $g_{s\ thermal}$ response curve was measured on a single leaf, acclimated to *PPFD*=750 µmol m^{-2} s^{-1} for 40 minutes, then *PPFD* was reduced by 90% for 60 minutes at t=0, indicated by an arrow. Values in the table are the mean of stomatal conductance traits for each accession. $t_{initial\ min}$ is in minutes, all other traits are dimensionless.

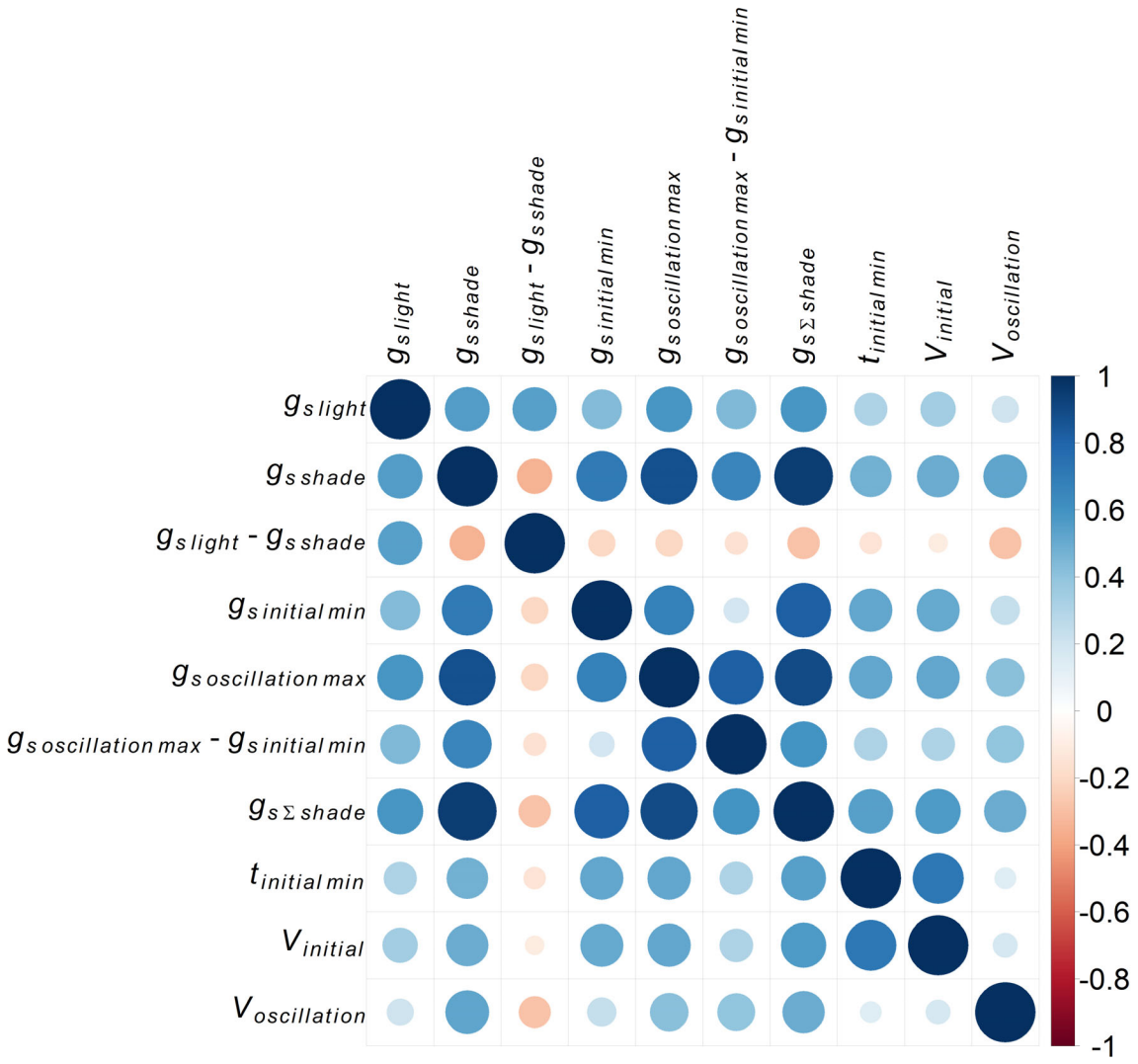

Figure 5: Pearson's correlation coefficients (*r*) between BLUPs of stomatal conductance traits. The size of circles indicates the strength of correlation, while color indicates whether the pairwise relationship was negative ($r<0$, red) or positive ($r>0$, blue). All corresponding scatterplots are given in Supplementary Fig. S1.

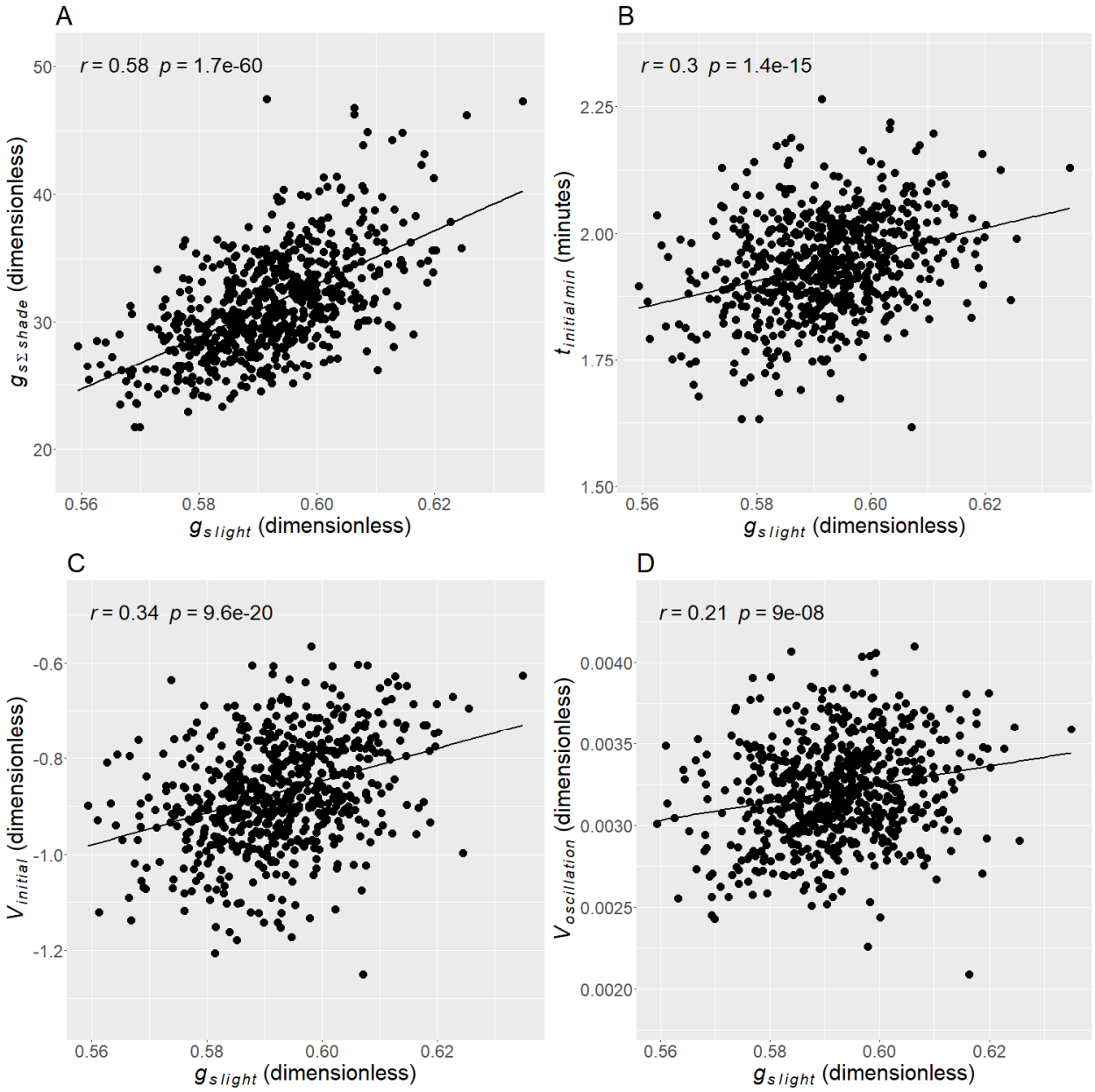

Figure 6: Correlation scatterplots between BLUPs for stomatal conductance traits. Pearson's *r* and the associated *p*-value are also given.

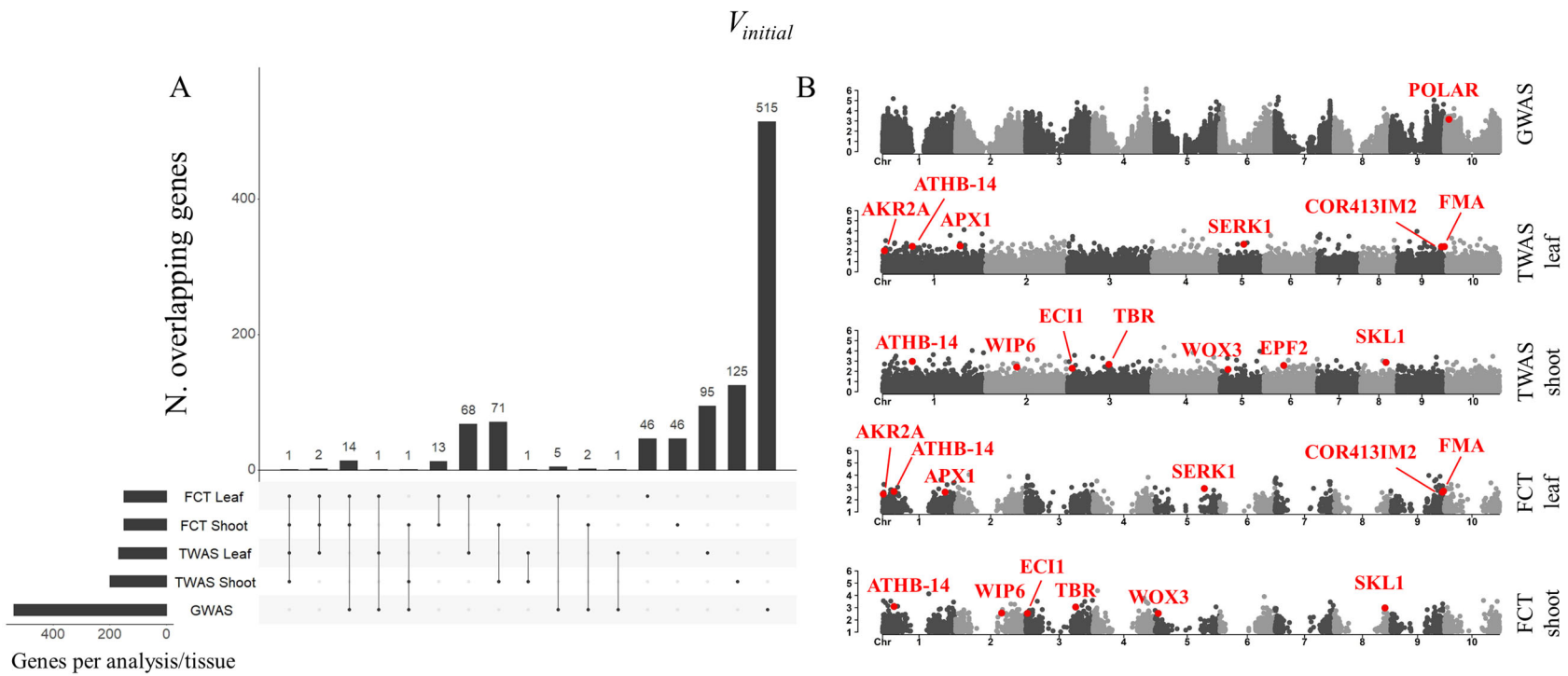

Figure 7: GWAS, TWAS and FCT results for $g_{s\ light}$. A: Upset plot showing the number of overlapping genes between the top hits in GWAS, TWAS leaf, TWAS shoot, FCT leaf, and/or FCT shoot. B: Manhattan plots of GWAS, TWAS and FCT results. Top hits are highlighted if they correspond to orthologues of known Arabidopsis stomatal genes (FMA, POLAR and EPF2, Table 3). Top hits are also highlighted if they are among the highest confidence genes identified by GWAS, TWAS, FCT, and subsequent GO enrichment analysis. (Supplementary Table S7). Equivalent figures for all other traits are in Supplemental Figures S2-12.

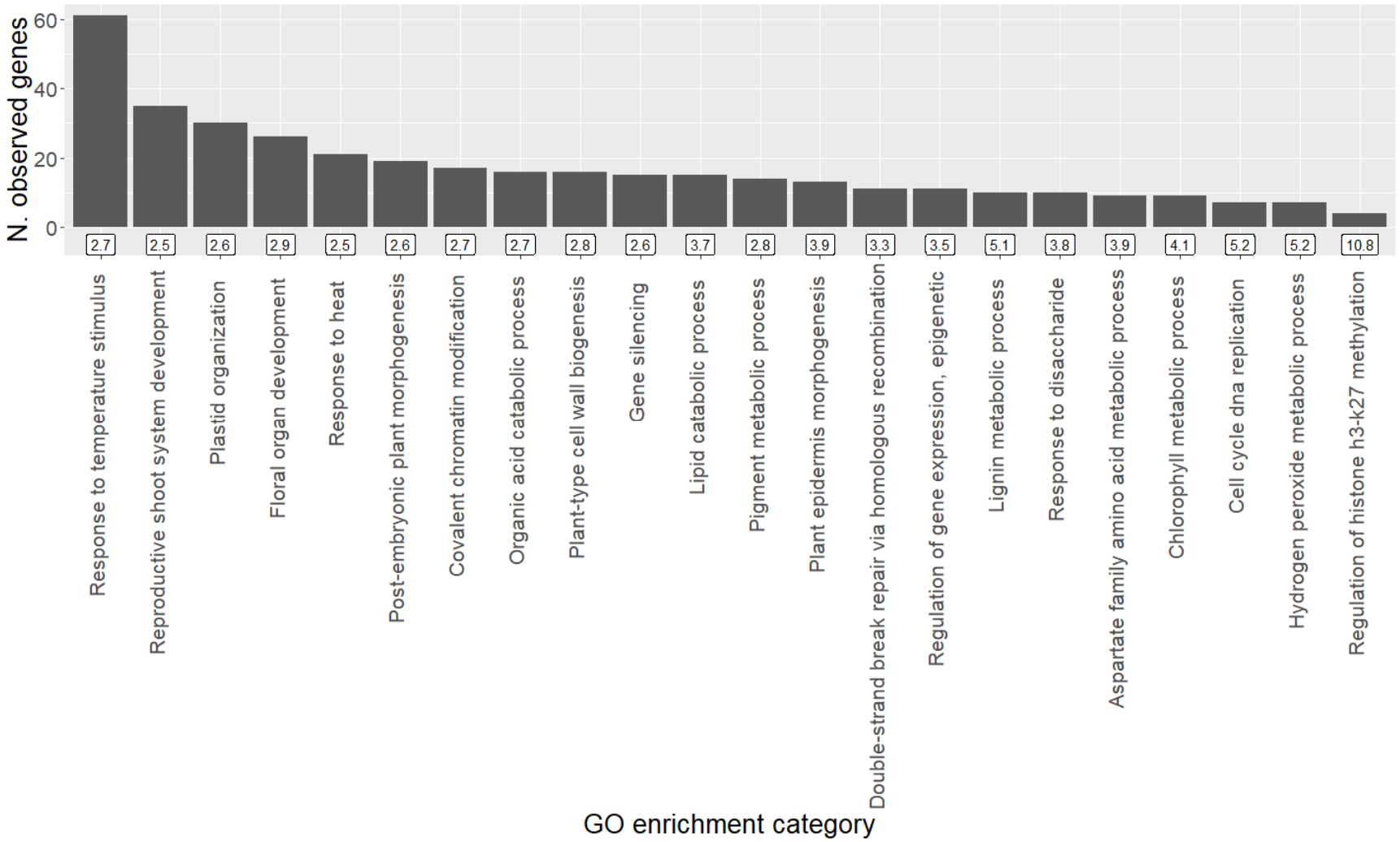

Figure 8: Results of GO enrichment analysis of higher confidence genes. Bars gives the number of genes included in each of the categories of GO biological processes that were significantly and >2.5-fold enriched. Fold-enrichment is shown in the label beneath each bar. Full GO enrichment analysis results are in Supplementary Table S6.

Parsed Citations

Acevedo-Siaca LG, Coe R, Wang Y, Kromdijk J, Quick WP, Long SP (2020) Variation in photosynthetic induction between rice accessions and its potential for improving productivity. New Phytologist: 12
Google Scholar: Author Only Title Only Author and Title

Ashburner M, Ball CA, Blake JA, Botstein D, Butler H, Cherry JM, Davis AP, Dolinski K, Dwight SS, Eppig JT, Harris MA, Hill DP, Issel-Tarver L, Kasarskis A, Lewis S, Matese JC, Richardson JE, Ringwald M, Rubin GM, Sherlock G, Gene Ontology C (2000) Gene Ontology: tool for the unification of biology. Nature Genetics 25: 25-29
Google Scholar: Author Only Title Only Author and Title

Assmann SM, Jegla T (2016) Guard cell sensory systems: recent insights on stomatal responses to light, abscisic acid, and CO2. Current Opinion in Plant Biology 33: 157-167
Google Scholar: Author Only Title Only Author and Title

Assmann SM, Shimazaki K (1999) The multisensory guard cell. Stomatal responses to blue light and abscisic acid. Plant Physiology 119: 809-815
Google Scholar: Author Only Title Only Author and Title

Ballard T, Peak D, Mott K (2019) Blue and red light effects on stomatal oscillations. Functional Plant Biology 46: 146-151
Google Scholar: Author Only Title Only Author and Title

Bartlett MK, Klein T, Jansen S, Choat B, Sack L (2016) The correlations and sequence of plant stomatal, hydraulic, and wilting responses to drought. Proceedings of the National Academy of Sciences of the United States of America 113: 13098-13103
Google Scholar: Author Only Title Only Author and Title

Bergmann DC, Lukowitz W, Somerville CR (2004) Stomatal development and pattern controlled by a MAPKK kinase. Science 304: 1494-1497
Google Scholar: Author Only Title Only Author and Title

Bernal-Vasquez AM, Utz HF, Piepho HP (2016) Outlier detection methods for generalized lattices: a case study on the transition from ANOVA to REML. Theoretical and Applied Genetics 129: 787-804
Google Scholar: Author Only Title Only Author and Title

Best NB, Hartwig T, Budka J, Fujioka S, Johal G, Schulz B, Dilkes BP (2016) nana plant2 Encodes a Maize Ortholog of the Arabidopsis Brassinosteroid Biosynthesis Gene DWARF1, Identifying Developmental Interactions between Brassinosteroids and Gibberellins. Plant Physiology 171: 2633-2647
Google Scholar: Author Only Title Only Author and Title

Bian C, Guo XY, Zhang Y, Wang L, Xu TD, DeLong A, Dong J (2020) Protein phosphatase 2A promotes stomatal development by stabilizing SPEECHLESS in Arabidopsis. Proceedings of the National Academy of Sciences of the United States of America 117: 13127-13137
Google Scholar: Author Only Title Only Author and Title

Boudolf V, Vlieghe K, Beemster GTS, Magyar Z, Acosta JAT, Maes S, Van Der Schueren E, INze D, De Veylder L (2004) The plant-specific cyclin-dependent kinase CDKB1;1 and transcription factor E2Fa-DPa control the balance of mitotically dividing and endoreduplicating cells in Arabidopsis. Plant Cell 16: 2683-2692
Google Scholar: Author Only Title Only Author and Title

Boyer JS (1982) Plant productivity and environment. Science 218: 443-448
Google Scholar: Author Only Title Only Author and Title

Bradbury PJ, Zhang Z, Kroon DE, Casstevens TM, Ramdoss Y, Buckler ES (2007) TASSEL: software for association mapping of complex traits in diverse samples. Bioinformatics 23: 2633-2635
Google Scholar: Author Only Title Only Author and Title

Browning BL, Browning SR (2016) Genotype Imputation with Millions of Reference Samples. American Journal of Human Genetics 98: 116-126
Google Scholar: Author Only Title Only Author and Title

Burks PS, Kaiser CM, Hawkins EM, Brown PJ (2015) Genomewide Association for Sugar Yield in Sweet Sorghum. Crop Science 55: 2138-2148
Google Scholar: Author Only Title Only Author and Title

Butler DG, Cullis BR, Gilmour AR, Gogel BJ (2009) ASReml-R reference manual. The State of Queensland, Department of Primary Industries and Fisheries, Brisbane .
Google Scholar: Author Only Title Only Author and Title

Carbon S, Douglass E, Dunn N, Good B, Harris NL, Lewis SE, Mungall CJ, Basu S, Chisholm RL, Dodson RJ, Hartline E, Fey P, Thomas PD, Albou LP, Ebert D, Kesling MJ, Mi H, Muruganujian A, Huang X, Poudel S, Mushayahama T, Hu JC, LaBonte SA, Siegele DA, Antonazzo G, Attrill H, Brown NH, Fexova S, Garapati P, Jones TEM, Marygold SJ, Millburn GH, Rey AJ, Trovisco V, dos Santos G, Emmert DB, Falls K, Zhou P, Goodman JL, Strelets VB, Thurmond J, Courtot M, Osumi-Sutherland D, Parkinson H, Roncaglia P,

Acencio ML, Kuiper M, Laegreid A, Logie C, Lovering RC, Huntley RP, Denny P, Campbell NH, Kramarz B, Acquaah V, Ahmad SH, Chen H, Rawson JH, Chibucos MC, Giglio M, Nadendla S, Tauber R, Duesbury MJ, Del-Toro N, Meldal BHM, Perfetto L, Porras P, Orchard S, Shrivastava A, Xie Z, Chang HY, Finn RD, Mitchell AL, Rawlings ND, Richardson L, Sangrador-Vegas A, Blake JA, Christie KR, Dolan ME, Drabkin HJ, Hill DP, Ni L, Sitnikov D, Harris MA, Oliver SG, Ruther-Ford K, Wood V, Hayles J, Bahler J, Lock A, Bolton ER, De Pons J, Dwinell M, Hayman GT, Laulederkind SJF, Shimoyama M, Tutaj M, Wang SJ, D'Eustachio P, Matthews L, Balhoff JP, Aleksander SA, Binkley G, Dunn BL, Cherry JM, Engel SR, Gondwe F, Karra K, MacPherson KA, Miyasato SR, Nash RS, Ng PC, Sheppard TK, Shrivatsav VPA, Simison M, Skrzypek MS, Weng S, Wong ED, Feuermann M, Gaudet P, Bakker E, Berardini TZ, Reiser L, Subramaniam S, Huala E, Arighi C, Auchincloss A, Axelsen K, Argoud-Puy G, Bateman A, Bely B, Blatter MC, Boutet E, Breuza L, Bridge A, Britto R, Bye-A-Jee H, Casals-Casas C, Coudert E, Estreicher A, Famiglietti L, Garmiri P, Georghiou G, Gos A, Gruaz-Gumowski N, Hatton-Ellis E, Hinz U, Hulo C, Ignatchenko A, Jungo F, Keller G, Laiho K, Lemercier P, Lieberherr D, Lussi Y, Mac-Dougall A, Magrane M, Martin MJ, Masson P, Natale DA, Hyka-Nouspikel N, Pedruzzi I, Pichler K, Poux S, Rivoire C, Rodriguez-Lopez M, Sawford T, Speretta E, Shypitsyna A, Stutz A, Sundaram S, Tognolli M, Tyagi N, Warner K, Zaru R, Wu C, Diehl AD, Chan J, Cho J, Gao S, Grove C, Harrison MC, Howe K, Lee R, Mendel J, Muller HM, Raciti D, Van Auken K, Berriman M, Stein L, Sternberg PW, Howe D, Toro S, Westerfield M, Gene Ontology C (2019) The Gene Ontology Resource: 20 years and still GOing strong. Nucleic Acids Research 47: D330-D338
Google Scholar: Author Only Title Only Author and Title

Casa AM, Pressoir G, Brown PJ, Mitchell SE, Rooney WL, Tuinstra MR, Franks CD, Kresovich S (2008) Community resources and strategies for association mapping in sorghum. Crop Science 48: 30-40
Google Scholar: Author Only Title Only Author and Title

Cernac A, Benning C (2004) WRINKLED1 encodes an AP2/EREB domain protein involved in the control of storage compound biosynthesis in Arabidopsis. Plant Journal 40: 575-585
Google Scholar: Author Only Title Only Author and Title

Chakravorty D, Gookin TE, Milner MJ, Yu YQ, Assmann SM (2015) Extra-Large G Proteins Expand the Repertoire of Subunits in Arabidopsis Heterotrimeric G Protein Signaling. Plant Physiology 169: 512-+
Google Scholar: Author Only Title Only Author and Title

Chang CC, Chow CC, Tellier L, Vattikuti S, Purcell SM, Lee JJ (2015) Second-generation PLINK: rising to the challenge of larger and richer datasets. Gigascience 4: 16
Google Scholar: Author Only Title Only Author and Title

Chater CCC, Caine RS, Fleming AJ, Gray JE (2017) Origins and Evolution of Stomatal Development. Plant Physiology 174: 624-638
Google Scholar: Author Only Title Only Author and Title

Chen L, Guan LP, Qian PP, Xu F, Wu ZL, Wu YJ, He K, Gou XP, Li J, Hou SW (2016) NRPB3, the third largest subunit of RNA polymerase II, is essential for stomatal patterning and differentiation in Arabidopsis. Development 143: 1600-1611
Google Scholar: Author Only Title Only Author and Title

Cominelli E, Galbiati M, Vavasseur A, Conti L, Sala T, Vuylsteke M, Leonhardt N, Dellaporta SL, Tonelli C (2005) A guard-cell-specific MYB transcription factor regulates stomatal movements and plant drought tolerance. Current Biology 15: 1196-1200
Google Scholar: Author Only Title Only Author and Title

de los Campos G, Sorensen D, Gianola D (2015) Genomic Heritability: What Is It? Plos Genetics 11: 21

De Souza AP, Wang Y, Orr DJ, Carmo-Silva E, Long SP (2020) Photosynthesis across African cassava germplasm is limited by Rubisco and mesophyll conductance at steady state, but by stomatal conductance in fluctuating light. New Phytologist 225: 2498-2512
Google Scholar: Author Only Title Only Author and Title

Deans RM, Brodribb TJ, Busch FA, Farquhar GD (2019) Plant water-use strategy mediates stomatal effects on the light induction of photosynthesis. New Phytologist 222: 382-395
Google Scholar: Author Only Title Only Author and Title

DeLucia EH, Chen S, Guan K, Peng B, Li Y, Gomez-Casanovas N, Kantola IB, Bernacchi CJ, Huang Y, Long SP, Ort DR (2019) Are we approaching a water ceiling to maize yields in the United States? Ecosphere 10(6)

dos Santos JPR, Fernandes SB, McCoy S, Lozano R, Brown PJ, Leakey ADB, Buckler ES, Garcia AAF, Gore MA (2020) Novel Bayesian Networks for Genomic Prediction of Developmental Traits in Biomass Sorghum. G3-Genes Genomes Genetics 10: 769-781
Google Scholar: Author Only Title Only Author and Title

Doyle J, Doyle J (1987) A rapid procedure for DNA purification from small quantities of fresh leaf tissue. . Phytochemical Bulletin 19: 11-15
Google Scholar: Author Only Title Only Author and Title

Durand M, Brendel O, Bure C, Le Thiec D (2019) Altered stomatal dynamics induced by changes in irradiance and vapour-pressure deficit under drought: impacts on the whole-plant transpiration efficiency of poplar genotypes. New Phytologist 222: 1789-1802
Google Scholar: Author Only Title Only Author and Title

Edwards EJ, Osborne CP, Stromberg CAE, Smith SA, Bond WJ, Christin PA, Cousins AB, Duvall MR, Fox DL, Freckleton RP, Ghannoum O, Hartwell J, Huang YS, Janis CM, Keeley JE, Kellogg EA, Knapp AK, Leakey ADB, Nelson DM, Saarela JM, Sage RF, Sala OE, Salamin N, Still CJ, Tipple B, Consortium CG (2010) The Origins of C4 Grasslands: Integrating Evolutionary and Ecosystem Science. Science 328: 587-591
Google Scholar: Author Only Title Only Author and Title

Elshire RJ, Glaubitz JC, Sun Q, Poland JA, Kawamoto K, Buckler ES, Mitchell SE (2011) A Robust, Simple Genotyping-by-Sequencing (GBS) Approach for High Diversity Species. Plos One 6: 10
Google Scholar: Author Only Title Only Author and Title

Endelman JB, Jannink JL (2012) Shrinkage Estimation of the Realized Relationship Matrix. G3-Genes Genomes Genetics 2: 1405-1413
Google Scholar: Author Only Title Only Author and Title

FAO, IFAD, UNICEF, WFP, WHO (2018) The State of Food Security and Nutrition in the World 2018. Building climate resilience for food security and nutrition. In. FAO, Rome, p 202
Google Scholar: Author Only Title Only Author and Title

Faralli M, Matthews J, Lawson T (2019) Exploiting natural variation and genetic manipulation of stomatal conductance for crop improvement. Current Opinion in Plant Biology 49: 1-7
Google Scholar: Author Only Title Only Author and Title

Ferguson JF, Fernandes SB, Monier B, Miller ND, Allen D, Dmitrieva, Schmuker P, Lozano R, Valluru R, Buckler ES, Gore MA, Brown PJ, Spalding EP, Leakey ADB (2020) Machine learning enabled phenotyping for GWAS and TWAS of WUE traits in 869 field-grown sorghum accessions. BioRXiv https://www.biorxiv.org/content/10.1101/2020.11.02.365213v1
Google Scholar: Author Only Title Only Author and Title

Filzmoser P, Garrett RG, Reimann C (2005) Multivariate outlier detection in exploration geochemistry. Computers & Geosciences 31: 579-587
Google Scholar: Author Only Title Only Author and Title

Franks PJ, Farquhar GD (2007) The mechanical diversity of stomata and its significance in gas-exchange control. Plant Physiology 143: 78-87
Google Scholar: Author Only Title Only Author and Title

Glaubitz JC, Casstevens TM, Lu F, Harriman J, Elshire RJ, Sun Q, Buckler ES (2014) TASSEL-GBS: A High Capacity Genotyping by Sequencing Analysis Pipeline. Plos One 9: 11
Google Scholar: Author Only Title Only Author and Title

Goodstein DM, Shu SQ, Howson R, Neupane R, Hayes RD, Fazo J, Mitros T, Dirks W, Hellsten U, Putnam N, Rokhsar DS (2012) Phytozome: a comparative platform for green plant genomics. Nucleic Acids Research 40: D1178-D1186
Google Scholar: Author Only Title Only Author and Title

Grant OM, Chaves MM, Jones HG (2006) Optimizing thermal imaging as a technique for detecting stomatal closure induced by drought stress under greenhouse conditions. Physiologia Plantarum 127: 507-518
Google Scholar: Author Only Title Only Author and Title

Grant OM, Tronina L, Jones HG, Chaves MM (2007) Exploring thermal imaging variables for the detection of stress responses in grapevine under different irrigation regimes. Journal of Experimental Botany 58: 815-825
Google Scholar: Author Only Title Only Author and Title

Guilioni L, Jones HG, Leinonen I, Lhomme JP (2008) On the relationships between stomatal resistance and leaf temperatures in thermography. Agricultural and Forest Meteorology 148: 1908-1912
Google Scholar: Author Only Title Only Author and Title

Głowacka K, Kromdijk J, Kucera K, Xie J, Cavanagh AP, Leonelli L, Leakey ADB, Ort DR, Niyogi KK, Long SP (2018) Photosystem II Subunit S overexpression increases the efficiency of water use in a field-grown crop. Nature Communications 9: 868
Google Scholar: Author Only Title Only Author and Title

Hadebe ST, Modi AT, Mabhaudhi T (2017) Drought Tolerance and Water Use of Cereal Crops: A Focus on Sorghum as a Food Security Crop in Sub-Saharan Africa. Journal of Agronomy and Crop Science 203: 177-191
Google Scholar: Author Only Title Only Author and Title

Hetherington AM, Woodward FI (2003) The role of stomata in sensing and driving environmental change. Nature 424: 901-908
Google Scholar: Author Only Title Only Author and Title

Jones HG (1999) Use of infrared thermometry for estimation of stomatal conductance as a possible aid to irrigation scheduling. Agricultural and Forest Meteorology 95: 139-149
Google Scholar: Author Only Title Only Author and Title

Jones HG, Stoll M, Santos T, de Sousa C, Chaves MM, Grant OM (2002) Use of infrared thermography for monitoring stomatal closure in the field: application to grapevine. Journal of Experimental Botany 53: 2249-2260
Google Scholar: Author Only Title Only Author and Title

Kaiser E, Morales A, Harbinson J (2018) Fluctuating Light Takes Crop Photosynthesis on a Rollercoaster Ride. Plant Physiology 176: 977-989
Google Scholar: Author Only Title Only Author and Title

Kaiser E, Morales A, Harbinson J, Kromdijk J, Heuvelink E, Marcelis LFM (2015) Dynamic photosynthesis in different environmental conditions. Journal of Experimental Botany 66: 2415-2426

Google Scholar: Author Only Title Only Author and Title

Kaiser H, Kappen L (2001) Stomatal oscillations at small apertures: indications for a fundamental insufficiency of stomatal feedback-control inherent in the stomatal turgor mechanism. Journal of Experimental Botany 52: 1303-1313
Google Scholar: Author Only Title Only Author and Title

Kang J, Hwang JU, Lee M, Kim YY, Assmann SM, Martinoia E, Lee Y (2010) PDR-type ABC transporter mediates cellular uptake of the phytohormone abscisic acid. Proceedings of the National Academy of Sciences of the United States of America 107: 2355-2360
Google Scholar: Author Only Title Only Author and Title

Kerstiens G (1996) Cuticular water permeability and its physiological significance. Journal of Experimental Botany 47: 1813-1832
Google Scholar: Author Only Title Only Author and Title

Kim CM, Dolan L (2011) Root hair development involves asymmetric cell division in Brachypodium distachyon and symmetric division in Oryza sativa. New Phytologist 192:601-610
Google Scholar: Author Only Title Only Author and Title

Klermund C, Ranftl QL, Diener J, Bastakis E, Richter R, Schwechheimer C (2016) LLM-Domain B-GATA Transcription Factors Promote Stomatal Development Downstream of Light Signaling Pathways in Arabidopsis thaliana Hypocotyls. Plant Cell 28: 646-660
Google Scholar: Author Only Title Only Author and Title

Koester RP, Nohl BM, Diers BW, Ainsworth EA (2016) Has photosynthetic capacity increased with 80 years of soybean breeding? An examination of historical soybean cultivars. Plant Cell and Environment 39: 1058-1067
Google Scholar: Author Only Title Only Author and Title

Kremling KAG, Diepenbrock CH, Gore MA, Buckler ES, Bandillo NB (2019) Transcriptome-Wide Association Supplements Genome-Wide Association in Zea mays. G3-Genes Genomes Genetics 9: 3023-3033
Google Scholar: Author Only Title Only Author and Title

Langmead B, Salzberg SL (2012) Fast gapped-read alignment with Bowtie 2. Nature Methods 9: 357-U354
Google Scholar: Author Only Title Only Author and Title

Lawson T, Blatt MR (2014) Stomatal Size, Speed, and Responsiveness Impact on Photosynthesis and Water Use Efficiency. Plant Physiology 164: 1556-1570
Google Scholar: Author Only Title Only Author and Title

Lawson T, Vialet-Chabrand S (2019) Speedy stomata, photosynthesis and plant water use efficiency. New Phytologist 221: 93-98
Google Scholar: Author Only Title Only Author and Title

Lawson T, von Caemmerer S, Baroli I (2011) Photosynthesis and Stomatal Behaviour. In U Luttge, W Beyschlag, B Budel, D Francis, eds, Progress in Botany 72, Vol 72. Springer-Verlag Berlin, Berlin, pp 265-304
Google Scholar: Author Only Title Only Author and Title

Le J, Liu XG, Yang KZ, Chen XL, Zou JJ, Wang HZ, Wang M, Vanneste S, Morita M, Tasaka M, Ding ZJ, Friml J, Beeckman T, Sack F (2014) Auxin transport and activity regulate stomatal patterning and development. Nature Communications 5
Google Scholar: Author Only Title Only Author and Title

Leakey ADB, Ferguson JN, Pignon CP, Wu A, Jin Z, Hammer GL, Lobell DB (2019) Water use efficiency as a constraint and target for improving the resilience and productivity of C3 and C4 crops. Annual Review of Plant Biology 70: 781-808
Google Scholar: Author Only Title Only Author and Title

Liu HJ, Yan JB (2019) Crop genome-wide association study: a harvest of biological relevance. Plant Journal 97: 8-18
Google Scholar: Author Only Title Only Author and Title

Lobell DB, Burke MB, Tebaldi C, Mastrandrea MD, Falcon WP, Naylor RL (2008) Prioritizing climate change adaptation needs for food security in 2030. Science 319: 607-610
Google Scholar: Author Only Title Only Author and Title

Lobell DB, Roberts MJ, Schlenker W, Braun N, Little BB, Rejesus RM, Hammer GL (2014) Greater Sensitivity to Drought Accompanies Maize Yield Increase in the US Midwest. Science 344: 516-519
Google Scholar: Author Only Title Only Author and Title

McAusland L, Davey PA, Kanwal N, Baker NR, Lawson T (2013) A novel system for spatial and temporal imaging of intrinsic plant water use efficiency. Journal of Experimental Botany 64: 4993-5007
Google Scholar: Author Only Title Only Author and Title

McAusland L, Vialet-Chabrand S, Davey P, Baker NR, Brendel O, Lawson T (2016) Effects of kinetics of light-induced stomatal responses on photosynthesis and water-use efficiency. New Phytologist 211: 1209-1220
Google Scholar: Author Only Title Only Author and Title

McLachlan DH, Lan J, Geilfus CM, Dodd AN, Larson T, Baker A, Horak H, Kollist H, He ZS, Graham I, Mickelbart MV, Hetherington AM (2016) The Breakdown of Stored Triacylglycerols Is Required during Light-Induced Stomatal Opening. Current Biology 26: 707-712
Google Scholar: Author Only Title Only Author and Title

Medlyn BE, Duursma RA, Eamus D, Ellsworth DS, Prentice IC, Barton CVM, Crous KY, de Angelis P, Freeman M, Wingate L (2011) Reconciling the optimal and empirical approaches to modelling stomatal conductance. Global Change Biology 17: 2134-2144
Google Scholar: Author Only Title Only Author and Title

Meng XZ, Chen X, Mang HG, Liu CL, Yu X, Gao XQ, Torii KU, He P, Shan LB (2015) Differential Function of Arabidopsis SERK Family Receptor-like Kinases in Stomatal Patterning. Current Biology 25: 2361-2372
Google Scholar: Author Only Title Only Author and Title

Merlot S, Mustilli AC, Genty B, North H, Lefebvre V, Sotta B, Vavasseur A, Giraudat J (2002) Use of infrared thermal imaging to isolate Arabidopsis mutants defective in stomatal regulation. Plant Journal 30: 601-609
Google Scholar: Author Only Title Only Author and Title

Mi HY, Muruganujan A, Ebert D, Huang XS, Thomas PD (2019) PANTHER version 14: more genomes, a new PANTHER GO-slim and improvements in enrichment analysis tools. Nucleic Acids Research 47: D419-D426
Google Scholar: Author Only Title Only Author and Title

Morris GP, Ramu P, Deshpande SP, Hash CT, Shah T, Upadhyaya HD, Riera-Lizarazu O, Brown PJ, Acharya CB, Mitchell SE, Harriman J, Glaubitz JC, Buckler ES, Kresovich S (2013) Population genomic and genome-wide association studies of agroclimatic traits in sorghum. Proceedings of the National Academy of Sciences of the United States of America 110: 453-458
Google Scholar: Author Only Title Only Author and Title

Ohashi-Ito K, Bergmann DC (2006) Arabidopsis FAMA controls the final proliferation/differentiation switch during stomatal development. Plant Cell 18: 2493-2505
Google Scholar: Author Only Title Only Author and Title

Ort DR, Long SP (2014) Limits on Yields in the Corn Belt. Science 344: 483-484
Google Scholar: Author Only Title Only Author and Title

Ortiz D, Hu JY, Fernandez MGS (2017) Genetic architecture of photosynthesis in Sorghum bicolor under non-stress and cold stress conditions. Journal of Experimental Botany 68: 4545-4557
Google Scholar: Author Only Title Only Author and Title

Papanatsiou M, Petersen J, Henderson L, Wang Y, Christie JM, Blatt MR (2019) Optogenetic manipulation of stomatal kinetics improves carbon assimilation, water use, and growth. Science 363: 1456-+
Google Scholar: Author Only Title Only Author and Title

Paterson AH, Bowers JE, Bruggmann R, Dubchak I, Grimwood J, Gundlach H, Haberer G, Hellsten U, Mitros T, Poliakov A, Schmutz J, Spannagl M, Tang HB, Wang XY, Wicker T, Bharti AK, Chapman J, Feltus FA, Gowik U, Grigoriev IV, Lyons E, Maher CA, Martis M, Narechania A, Otillar RP, Penning BW, Salamov AA, Wang Y, Zhang LF, Carpita NC, Freeling M, Gingle AR, Hash CT, Keller B, Klein P, Kresovich S, McCann MC, Ming R, Peterson DG, Mehboob ur R, Ware D, Westhoff P, Mayer KFX, Messing J, Rokhsar DS (2009) The Sorghum bicolor genome and the diversification of grasses. Nature 457: 551-556
Google Scholar: Author Only Title Only Author and Title

Pearcy RW (1990) Sunflecks and photosynthesis in plant canopies. Annual Review of Plant Physiology and Plant Molecular Biology 41: 421-453
Google Scholar: Author Only Title Only Author and Title

Pena MJ, Zhong RQ, Zhou GK, Richardson EA, O'Neill MA, Darvill AG, York WS, Ye ZH (2007) Arabidopsis irregular xylem8 and irregular xylem9: Implications for the complexity of glucuronoxylan biosynthesis. Plant Cell 19: 549-563
Google Scholar: Author Only Title Only Author and Title

Petricka JJ, Clay NK, Nelson TM (2008) Vein patterning screens and the defectively organized tributaries mutants in Arabidopsis thaliana. Plant Journal 56: 251-263
Google Scholar: Author Only Title Only Author and Title

Pignon CP, Leakey ADB, Long SP, Kromdijk J (2021) Drivers of Natural Variation in Water-Use Efficiency Under Fluctuating Light Are Promising Targets for Improvement in Sorghum. Frontiers in Plant Science 12: 13
Google Scholar: Author Only Title Only Author and Title

Pillitteri LJ, Dong J (2013) Stomatal development in Arabidopsis. In, Ed e0162. BioOne, The Arabidopsis book, p e0162
Google Scholar: Author Only Title Only Author and Title

Pnueli L, Liang H, Rozenberg M, Mittler R (2003) Growth suppression, altered stomatal responses, and augmented induction of heat shock proteins in cytosolic ascorbate peroxidase (Apx1)-deficient Arabidopsis plants. Plant Journal 34: 187-203
Google Scholar: Author Only Title Only Author and Title

Portis AR (2003) Rubisco activase - Rubisco's catalytic chaperone. Photosynthesis Research 75: 11-27
Google Scholar: Author Only Title Only Author and Title

R Core Team (2017) R: A language and environment for statistical computing., R Foundation for Statistical Computing, Vienna, Australia

Raissig MT, Abrash E, Bettadapur A, Vogel JP, Bergmann DC (2016) Grasses use an alternatively wired bHLH transcription factor network to establish stomatal identity. Proceedings of the National Academy of Sciences of the United States of America 113: 8326-8331
Google Scholar: Author Only Title Only Author and Title

Ray DK, Mueller ND, West PC, Foley JA (2013) Yield Trends Are Insufficient to Double Global Crop Production by 2050. Plos One 8: 8
Google Scholar: Author Only Title Only Author and Title

Regassa TH, Wortmann CS (2014) Sweet sorghum as a bioenergy crop: Literature review. Biomass & Bioenergy 64: 348-355
Google Scholar: Author Only Title Only Author and Title

Remm M, Storm CEV, Sonnhammer ELL (2001) Automatic clustering of orthologs and in-paralogs from pairwise species comparisons. Journal of Molecular Biology 314: 1041-1052
Google Scholar: Author Only Title Only Author and Title

Sack L, Cowan PD, Jaikumar N, Holbrook NM (2003) The 'hydrology' of leaves: co-ordination of structure and function in temperate woody species. Plant Cell and Environment 26: 1343-1356
Google Scholar: Author Only Title Only Author and Title

Serna L (2011) Stomatal development in Arabidopsis and grasses: differences and commonalities. International Journal of Developmental Biology 55: 5-10
Google Scholar: Author Only Title Only Author and Title

Shimazaki K, Doi M, Assmann SM, Kinoshita T (2007) Light regulation of stomatal movement. Annual Review of Plant Biology 58: 219-247
Google Scholar: Author Only Title Only Author and Title

Sierla M, Waszczak C, Vahisalu T, Kangasjarvi J (2016) Reactive Oxygen Species in the Regulation of Stomatal Movements. Plant Physiology 171: 1569-1580
Google Scholar: Author Only Title Only Author and Title

Sinclair TR, Tanner CB, Bennett JM (1984) Water-use efficiency in crop production. Bioscience 34: 36-40
Google Scholar: Author Only Title Only Author and Title

Soleh MA, Tanaka Y, Nomoto Y, Iwahashi Y, Nakashima K, Fukuda Y, Long SP, Shiraiwa T (2016) Factors underlying genotypic differences in the induction of photosynthesis in soybean Glycine max (L.) Merr. Plant Cell and Environment 39: 685-693
Google Scholar: Author Only Title Only Author and Title

Stegle O, Parts L, Durbin R, Winn J (2010) A Bayesian Framework to Account for Complex Non-Genetic Factors in Gene Expression Levels Greatly Increases Power in eQTL Studies. Plos Computational Biology 6: 11
Google Scholar: Author Only Title Only Author and Title

Takahashi S, Monda K, Negi J, Konishi F, Ishikawa S, Hashimoto-Sugimoto M, Goto N, Iba K (2015) Natural Variation in Stomatal Responses to Environmental Changes among Arabidopsis thaliana Ecotypes. Plos One 10: 13
Google Scholar: Author Only Title Only Author and Title

Tam V, Patel N, Turcotte M, Bosse Y, Pare G, Meyre D (2019) Benefits and limitations of genome-wide association studies. Nature Reviews Genetics 20: 467-484
Google Scholar: Author Only Title Only Author and Title

Taylor SH, Hulme SP, Rees M, Ripley BS, Woodward FI, Osborne CP (2010) Ecophysiological traits in C3 and C4 grasses: a phylogenetically controlled screening experiment. New Phytologist 185: 780-791
Google Scholar: Author Only Title Only Author and Title

Valluru R, Gazave EE, Fernandes SB, Ferguson JN, Lozano R, Hirannaiah P, Zuo T, Brown PJ, Leakey ADB, Gore MA, Buckler ES, Bandillo N (2019) Deleterious Mutation Burden and Its Association with Complex Traits in Sorghum (Sorghum bicolor). Genetics 211: 1075-1087
Google Scholar: Author Only Title Only Author and Title

Vialet-Chabrand S, Lawson T (2019) Dynamic leaf energy balance: deriving stomatal conductance from thermal imaging in a dynamic environment. Journal of Experimental Botany 70: 2839-2855
Google Scholar: Author Only Title Only Author and Title

Vico G, Manzoni S, Palmroth S, Katul G (2011) Effects of stomatal delays on the economics of leaf gas exchange under intermittent light regimes. New Phytologist 192: 640-652
Google Scholar: Author Only Title Only Author and Title

von Caemmerer S, Farquhar GD (1981) Some relationships between the biochemistry of photosynthesis and the gas exchange of leaves. Planta 153: 376-387
Google Scholar: Author Only Title Only Author and Title

Waduwara-Jayabahu I, Oppermann Y, Wirtz M, Hull ZT, Schoor S, Plotnikov AN, Hell R, Sauter M, Moffatt BA (2012) Recycling of Methylthioadenosine Is Essential for Normal Vascular Development and Reproduction in Arabidopsis. Plant Physiology 158: 1728-1744
Google Scholar: Author Only Title Only Author and Title

Wang Y, Burgess SJ, de Becker EM, Long SHP (2020) Photosynthesis in the fleeting shadows: an overlooked opportunity for increasing crop productivity? Plant Journal 101: 874-884
Google Scholar: Author Only Title Only Author and Title

Wang YH, Xue XY, Zhu JK, Dong J (2016) Demethylation of ERECTA receptor genes by IBM1 histone demethylase affects stomatal development. Development 143: 4452-4461
Google Scholar: Author Only Title Only Author and Title

Way DA, Pearcy RW (2012) Sunflecks in trees and forests: from photosynthetic physiology to global change biology. Tree Physiology 32: 1066-1081
Google Scholar: Author Only Title Only Author and Title

Wei T, Simko V (2017) R package "corrplot": Visualization of a Correlation Matrix. In,
Google Scholar: Author Only Title Only Author and Title

Wong SC, Cowan IR, Farquhar GD (1979) Stomatal conductance correlates with photosynthetic capacity. Nature 282: 424-426
Google Scholar: Author Only Title Only Author and Title

WWAP (2015) The United Nations world water development report 2015: Water for a sustainable world. In. UNESCO, Paris
Google Scholar: Author Only Title Only Author and Title

Xie J, Mayfield-Jones D, Erice G, Choi M, Leakey ADB (2020) Optical topometry and machine learning to rapidly phenotype stomatal patterning traits for QTL mapping in maize. BioRXiv https://www.biorxiv.org/content/10.1101/2020.10.09.333880v1
Google Scholar: Author Only Title Only Author and Title

Yu HY, Murchie EH, Gonzalez-Carranza ZH, Pyke KA, Roberts JA (2015) Decreased photosynthesis in the erect panicle 3 (ep3) mutant of rice is associated with reduced stomatal conductance and attenuated guard cell development. Journal of Experimental Botany 66: 1543-1552
Google Scholar: Author Only Title Only Author and Title

Zhang YY, Zhu HY, Zhang Q, Li MY, Yan M, Wang R, Wang LL, Welti R, Zhang WH, Wang XM (2009) Phospholipase D alpha 1 and Phosphatidic Acid Regulate NADPH Oxidase Activity and Production of Reactive Oxygen Species in ABA-Mediated Stomatal Closure in Arabidopsis. Plant Cell 21: 2357-2377
Google Scholar: Author Only Title Only Author and Title

Zhou X, Stephens M (2012) Genome-wide efficient mixed-model analysis for association studies. Nature Genetics 44: 821-U136
Google Scholar: Author Only Title Only Author and Title

Zhou X, Stephens M (2014) Efficient multivariate linear mixed model algorithms for genome-wide association studies. Nature Methods 11: 407-+
Google Scholar: Author Only Title Only Author and Title

Zhou XY, Huang XH (2019) Genome-wide Association Studies in Rice: How to Solve the Low Power Problems? Molecular Plant 12: 10-12
Google Scholar: Author Only Title Only Author and Title

Zhu XG, Ort DR, Whitmarsh J, Long SP (2004) The slow reversibility of photosystem II thermal energy dissipation on transfer from high to low light may cause large losses in carbon gain by crop canopies: a theoretical analysis. Journal of Experimental Botany 55: 1167-1175
Google Scholar: Author Only Title Only Author and Title